Nanoscale

REVIEW

View Article Online
View Journal | View Issue

Check for updates

Cite this: *Nanoscale*, 2025, **17**, 9686

Self-assembled monolayer functionalized metal oxides: a path toward highly selective and low-power consuming gas sensors

Navpreet Kaur *†[a] and Mandeep Singh *†[b]

The emerging functionalization strategy of self-assembled monolayers (SAMs) offers transformative potential for enhancing the performance of nanostructured metal oxides (MOXs)-based gas sensors. Being a 2D-molecular arrangement with a unique structure, polar SAMs tend to modulate the surface charge density and offer distinct surface-specific interactions that lead to enhancement of the sensor performance. This review is focused on highlighting their potential and explores the advancements in SAM-functionalized MOXs, with a particular emphasis on 1D nanostructures such as nanowires and nanotubes. By tailoring the surface chemistry through SAM functionalization, these sensors achieve remarkable improvements in sensitivity, selectivity, and operational temperature, overcoming the persistent challenges of MOX sensors. In addition to the fundamental aspect of SAMs, recent progress in tuning the sensing performance of different 1D-nanostructured MOXs, including SnO_2, ZnO, WO_3, and NiO *via* SAM functionalization, is systematically reviewed. This review also discusses in detail the underlying sensing mechanism and key findings that underscore the ability of SAMs to offer selective interactions with gas analytes, helping to improve their response dynamics and enable low-temperature operation. Finally, the major challenges are addressed, providing a roadmap for future research. This review presents SAMs as a versatile platform for nanoscale functionalization, advancing the design of energy-efficient and high-performance gas sensors for environmental monitoring and healthcare.

Received 17th December 2024,
Accepted 18th March 2025

DOI: 10.1039/d4nr05307a

rsc.li/nanoscale

Open Access Article. Published on 20 bezna 2025. Downloaded on 29.05.2026 23:13:50.
This article is licensed under a Creative Commons Attribution 3.0 Unported Licence.

1. Introduction

The need for real-time, ultrasensitive monitoring of human and environmental health is becoming increasingly critical due to the continuous expansion of chemical industries, along with urbanization, climate change, and environmental pollution.[1,2] These necessities, combined with technological advancements such as artificial intelligence (AI) and the Internet of Things (IoT), drive the need of low-cost, chemically/physically stable and multifunctional advanced nanomaterials for the development of portable, energy-efficient sensing platforms.[3–8] Nanostructured metal oxides have long been recognized as a prominent choice in chemical/gas sensing applications due to their remarkable properties like high sensitivity, stability, versatility and, most importantly, the possibility to synthesize them in different nanostructured forms.[9–13] Among the various nanoscale morphologies of MOXs, one-dimensional (1D) nanostructures, such as nanowires and nanotubes, have gathered significant attention for sensing due to their unique and favorable properties apart from their high surface-to-volume ratio. These properties include fast response dynamics, well-defined crystal orientations, controlled unidirectional electrical properties, abundant active sites and direct electron transport pathways, which collectively enhance their ability to detect trace concentrations of gases with high sensitivity.[14] Despite these advantages, thin film- and nanostructure-based MOX sensors face persistent challenges of high operating temperatures and limited selectivity, which hinder their practicality for the next-generation low-power consuming sensors.[14–17] Addressing these challenges necessitates innovative strategies that leverage the inherent nanoscale properties of 1D MOX nanostructures to achieve superior sensing performance.

To tackle the issue of high-temperature operation, photoactivation (especially using ultraviolet (UV) light) has been proposed, exploiting the wide bandgap of MOXs in the UV region.[3,18–22] It has also been seen that MOX nanostructures showed photogeneration of charge carriers through absorption of two or more photons *via* illumination with visible light.[23–26] Additionally, degenerately doped MOX quantum dot nanocrys-

[a]*SENSOR Laboratory, Department of Information Engineering (DII), University of Brescia, Via D. Valotti 9, Brescia 25133, Italy. E-mail: navpreet.kaur@unibs.it*
[b]*IMEM-CNR Institute, Via alla Cascata 56/C, Povo-38123-Trento, Italy. E-mail: msingh@fbk.eu*
†These authors contributed equally to this work.

This journal is © The Royal Society of Chemistry 2025

Open Access Article. Published on 20 bezna 2025. Downloaded on 29.05.2026 23:13:50.
This article is licensed under a Creative Commons Attribution 3.0 Unported Licence.

tals exhibit localized surface plasmon resonance (LSPR) in the wide range of infrared (IR) region.[27–31] These unique light–matter interactions create the strong possibility to develop low-power consuming or room-temperature chemical/gas sensors based on nanostructured MOXs *via* harvesting energy from UV-Vis-IR light.[31,32] Even though photoactivated MOX sensors have shown promising results, selectivity remains a significant challenge, as gas analytes often exhibit overlapping adsorption behavior on MOX surfaces.[3]

In the MOXs, chemisorbed oxygen ions determine their sensing mechanisms, or in other words, decide the interactions with the gas analyte.[33–36] As the type of these chemisorbed oxygen ions depends on the operating temperature, one way to tune the selectivity is to operate the MOX sensor at different temperatures. However, one needs to operate the MOX sensor at a high temperature while sensing complex or particular gas analytes.[13] To tackle the issue of selectivity, numerous strategies have been employed to improve selectivity, including metal–particle decoration,[37–39] heterojunction formation,[40–42] and core–shell structures.[43–45] However, achieving consistent, tunable, and reproducible selectivity across a range of gas analytes remains an elusive goal.

In recent years, the surface functionalization of MOXs with self-assembled monolayers (SAMs) has emerged as a promising and versatile approach to overcome these limitations.[46–48] SAMs are highly ordered molecular assemblies that spontaneously form on surfaces, introducing specific functional groups to tailor surface chemistry and enhance sensor performance.[49] By enabling selective surface interactions and modulating charge density, SAMs address key challenges in MOX sensors, including selectivity and high-temperature operation.[50,51] The concept of SAM functionalization is well-established in electronic devices such as organic field-effect transistors (OFETs),[52–54] where SAMs are employed to modify injection barriers and improve charge transport. For instance, X. Cheng *et al*. have improved the performance of ambipolar OFET *via* functionalizing the gold (Au) electrode with SAMs that help improve the electron and hole injection barrier at the gold/semiconductor interface.[52] In biosensors, SAMs are extensively utilized to immobilize biomolecules, providing a bioreceptive interface that facilitates high selectivity.[49,55–57]

In the case of gas sensors, the initial exploration of SAM-functionalized MOX sensors began with the pioneering work by Hoffmann *et al*. in 2014,[48] where SAM-modified SnO_2 nanowires demonstrated the highly selective detection of NO_2 at room temperature using solar illumination instead of thermal activation. This innovation eliminated the need for thermal activation, highlighting the potential of SAMs to lower operational temperatures while maintaining high sensitivity and selectivity. Since then, research in this area has expanded, yet the body of work remains relatively limited, especially considering the potential of SAM functionalization as a versatile, tunable platform for gas sensing. Although SAMs have shown promising results with n-type MOXs, such as SnO_2,[48,58] ZnO,[46,59] and WO_3,[47,60] applications on p-type MOXs like NiO[50] are scarce, indicating a research gap that could unlock further advancements in low-temperature, selective gas sensors.

This review aims to provide a comprehensive overview of the recent progress in SAM-functionalized MOX-based gas sensors, with a specific focus on 1D nanostructures such as nanowires and nanotubes. The discussion begins with an overview of SAMs, including their molecular structure, formation processes on MOX surfaces, and their role in modulating surface charge density to enhance sensor performance. The subsequent sections systematically review the literature on

Navpreet Kaur

Dr Navpreet Kaur is a Postdoctoral Researcher at the University of Brescia, Italy, specializing in nanomaterials and chemical/gas sensors. With a Ph. D. in Physical Science and Engineering, she focuses on enhancing sensing performance through advanced material engineering, including metal oxide nanostructures, heterostructures and functionalization. Her current work involves the development of low-power consuming sensors using metal–organic framework functionalized nanowires for environmental and health monitoring. Dr Kaur has conducted international research at NTU-Singapore as a visiting researcher and is currently serving as an Early Career Editorial Board for Hygiene and Environmental Health Advances (Elsevier) and Guest Editor for Sensors (MDPI).

Mandeep Singh

Dr Mandeep Singh received his Ph.D. in Chemistry of Innovative Materials from the University of Bari, Italy. He pursued postdoctoral research at the University of Brescia and Politecnico di Milano and was a visiting researcher at the University of Texas at Austin. In 2024, he joined IMEM-CNR, Trento, as a Researcher (Level III). His research spans the development of high-k material thin films via PE-ALD for microelectronics, SAM-functionalized metal oxide nanostructures for VOC detection, and the synthesis and ultrafast spectroscopic investigation of excitonic and plasmonic dynamics in heavily doped colloidal nanocrystals. He also served as a Guest Editor for MDPI Sensors.

Open Access Article. Published on 20 bezna 2025. Downloaded on 29.05.2026 23:13:50.
This article is licensed under a Creative Commons Attribution 3.0 Unported Licence.

SAM-functionalized MOXs, emphasizing the formation processes, sensor device performance, and underlying sensing mechanisms. Finally, the review concludes with a discussion of challenges, limitations, and future perspectives to inspire further research in this promising field.

2. Self-assembled monolayers: structure, formation on MOXs surface and surface charge modulation using polar SAMs

2.1. Structure to SAM

Being an unifying concept in nature, SAMs can be formed on a variety of surfaces, including metal oxides,[61] organic semiconductors,[62] and polymers,[63] thereby creating chemically active interfaces.[49] SAM formation is a "bottom-up" approach, in which a monolayer is assembled molecule by molecule, enabling the construction of unique and novel molecular architectures.[49] Structurally, SAMs consist of three main components (Fig. 1, left):

2.1.1. Head group. Responsible for binding to the surface.

2.1.2. Backbone. An aromatic oligomer or aliphatic chain that connects the head and terminal groups while defining molecular ordering.

2.1.3. Terminal group. Governs the surface functionality, topography, and surface energy of the functionalized surface.

In chemical sensing applications, the terminal group of a SAM is crucial for determining sensor performance and surface functionality.[49] For biosensors, SAMs formed on the active sensing layer act as mediators for immobilizing biomolecules, providing a bio-receptive platform where the terminal SAM molecules interact with the biomolecules.[61,64,65] For example, to detect the odorant binding protein (OBP) chiral interactions *via* the electrolyte-gated organic field effect transistor (EG-OFET), the gold gate electrode is first functionalized with a 3-mercaptopropionic acid (3MPA) SAM to immobilize porcine OBP.[66] In gas sensors, which are the focus of this review, SAMs with polar terminal groups (electron-donating or electron-withdrawing) modulate the surface charge of the active layer,[67] enhancing the sensitivity, selectivity, and operating temperature.[46,51,59] Additionally, the terminal group undergoes surface-specific interactions with gas analytes to facilitate selective detection and improve the overall sensor performance.[46,50,51,58]

For a detailed discussion on the fundamental principles of SAM formation, readers may refer to Ulman's comprehensive review.[68] Meanwhile, for a more experimental perspective that covers SAM formation, critical factors affecting their formation and functionality, and their applications in modern electronic devices such as sensors, readers can refer to our previous review article.[49]

2.2. SAMs formation on MOXs surface

Even though surface functionalization of MOXs were done with different types of SAM molecules like phosphonic acid,[61] organosilanes such as (3-aminopropyl)trimethoxysilane (APTES or APTMS) are widely used in enhancing and tuning the sensing performance of MOXs. Thus, in this article, we will focus mainly on the formation of organosilanes on MOXs surfaces. These SAMs require hydroxyl groups (–OH) on the MOX surface to facilitate the binding. This approach falls under the category of "surface decoupled" formation, as the attachment of SAMs occurs through reactions with –OH groups, rather than direct bonding to the specific substrate sites.[69] While in the case of "surface coupled" formation, a direct binding occurs between the SAM head group and the surface, *e.g.*, the formation of thiols with gold (Au).[70]

Organosilanes are monomeric silicon-based compounds containing both head and terminal functional groups connected by a silicon atom.[71] For instance, the chemical structure of APTES includes a head group ($-CH_3$) and a terminal group ($-NH_2$), as shown in Fig. 1 (right). The surface –OH groups can be introduced by treatments such as oxygen plasma, piranha solution, or UV illumination on the MOXs surface.[49] The process of attachment of APTES with the MOX nanowires is shown in Fig. 2, along with a mediating step for obtaining –OH groups on MOXs. Different methods have been used in the literature to functionalize the surface of MOXs

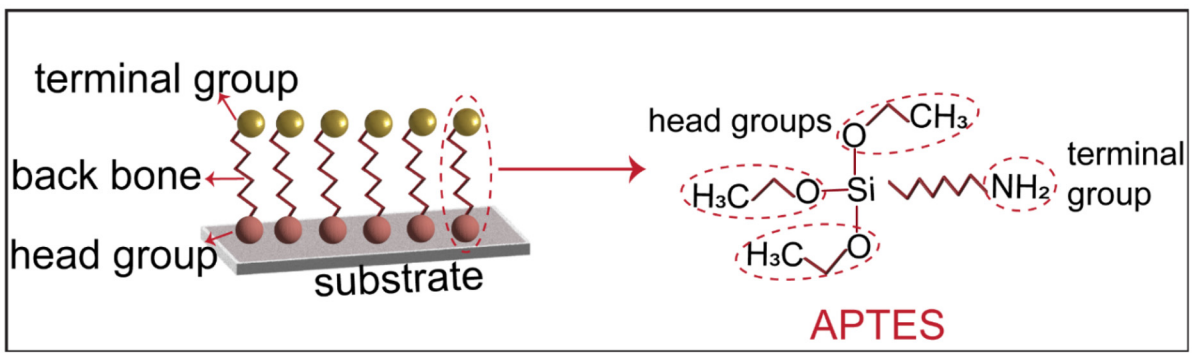

Fig. 1 Chemical structure of APTES showing the head and terminal functional groups.

This journal is © The Royal Society of Chemistry 2025

Open Access Article. Published on 20 bezna 2025. Downloaded on 29.05.2026 23:13:50.
This article is licensed under a Creative Commons Attribution 3.0 Unported Licence.

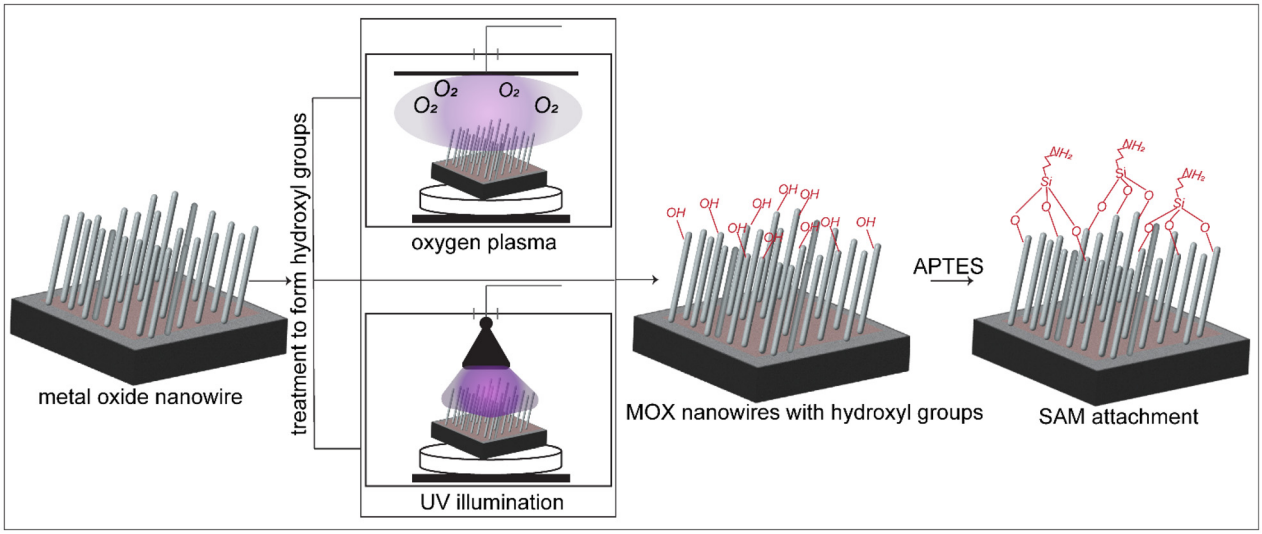

Fig. 2 Attachment of SAM on the MOX surface.

with organosilanes, but the most common ones are chemical vapor deposition CVD[60] and dip method.[46,59]

2.2.1. Dip method. In this method, the desired molar concentration of the organosilane solution is prepared in a solvent like ethanol.[46,59] The substrate to be functionalized is dipped inside this solution for a prolonged duration. During SAM formation, the head functional groups of organosilanes undergo hydrolysis, condensation, and covalent bonding with the –OH groups on the MOX surface, leading to the formation of a stable polysiloxane network. Kinetically, SAM formation proceeds in two stages. The initial stage is rapid, lasting only a few minutes, during which the monolayer forms through the adsorption of SAM molecules onto the surface. The second stage involves achieving ordering within the monolayer *via* molecular rearrangement and reorientation. This stage typically lasts 10–20 hours. However, many reports can be found in the literature where the SAM formation process is relatively complete within a shorter duration.[49] Once the SAM formation is complete, the samples are removed from the solution and thoroughly rinsed with the solvent to eliminate any unbound or surface-adsorbed residual SAM molecules.

Additionally, mixed SAMs can be formed by combining two types of organosilanes in the solution, allowing for more complex surface functionalities. An example of mono- and mixed SAM formation using APTES and tetraethyl orthosilicate (TEOS) on ZnO nanowire surfaces is shown in Fig. 3.[51]

2.2.2. Chemical vapor deposition (CVD). In the CVD method, organosilane precursors are vaporized and delivered to the MOX surface under controlled temperature and pressure conditions.[72–75] The vaporized molecules react with the hydroxyl (–OH) groups present on the surface, forming covalent bonds and creating a uniform monolayer.[76] This technique typically operates at elevated temperatures, which facilitate the hydrolysis and condensation reactions required for SAM formation. During the process, the reaction chamber is purged with inert gases like nitrogen or argon to ensure a clean environment and prevent unwanted reactions. The uniformity of the SAM layers achieved *via* CVD is superior to that of solution-based methods, making it suitable for applications

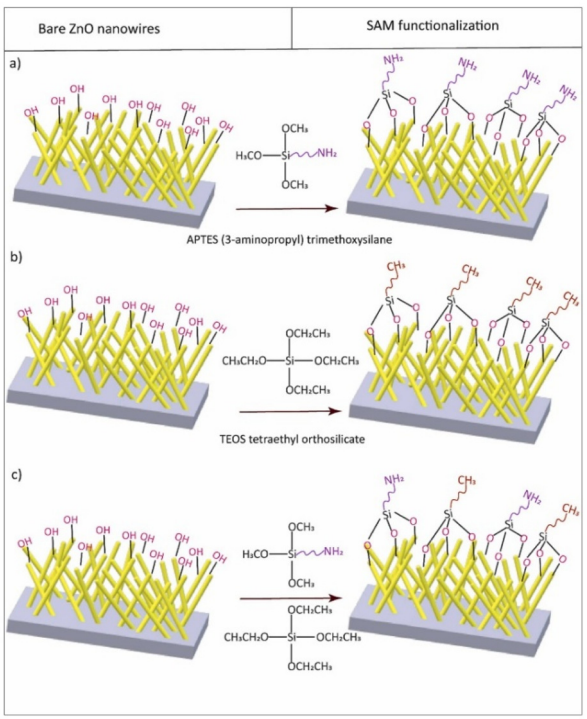

Fig. 3 Functionalization strategy of ZnO nanowires with homogeneous SAMs of APTES (a) and TEOS (b) monolayers, which leads to the formation of amine ($-NH_2$) and methyl ($-CH_3$) terminated ZnO nanowires, respectively. In panel c, ZnO nanowires were functionalized with a mixture of APTES and TEOS monolayers in a different ratio. Reproduced from ref. 51 with permission from Elsevier B.V., copyright 2023.

Open Access Article. Published on 20 bezna 2025. Downloaded on 29.05.2026 23:13:50.
This article is licensed under a Creative Commons Attribution 3.0 Unported Licence.

requiring precise control over surface properties. While CVD is highly effective for producing high-purity SAM layers, it often requires specialized equipment and careful optimization of parameters such as precursor flow rate, substrate temperature, and chamber pressure.

Each technique offers unique benefits, with dip-coating being the most accessible for research and initial studies,[49] while CVD provides superior uniformity and scalability for advanced applications[72,76,77] The choice of method significantly impacts the quality, stability, and functional properties of the SAM layer, which, in turn, influences the sensor performance in terms of the sensitivity, selectivity, and operational stability. Table 1 represents the advantages and disadvantages of each technique for clear observation.

2.3. Modulation of the surface charge using polar SAMs

A key question in gas sensing is how surface functionalization with SAMs enhances the sensor performance. One illustrative example is provided by S. Kobayashi *et al.*,[67] who demonstrated that the modulation of the surface carrier density in organic field-effect transistors (OFETs) can tune device performance. In this work, the surface of p-type (pentacene) and n-type (fullerene, C_{60}) based OFET devices were functionalized with three different types of organosilanes: $(CF_3)(CF_2)_7(CH_2)_2Si(OC_2H_5)_3$, $(CH_3)(CH_2)_7Si(OC_2H_5)_3$ and $(NH_2)(CH_2)_3Si(OC_2H_5)_3$. However, here we will focus mainly on $(CF_3)(CF_2)_7(CH_2)_2Si(OC_2H_5)_3$ and $(NH_2)(CH_2)_3Si(OC_2H_5)_3$, as these SAMs significantly influence the performance of OFET. The main functional property of both these SAMs that need to be noted is the polarities of terminal groups: CF_3 is electron withdrawing, and NH_2 is electron donating.

The SAM with CF_3 terminal group was formed using the CVD method, while the NH_2-terminated SAM was applied using the dip method. OFET characteristics show that beside the modulation in the drain current after the functionalization, a major effect was observed in the threshold voltage (V_{th}) shift, which is shown in Fig. 4 for both types of OFET. Particularly, CF_3 or F-SAM tends to shift the V_{th} to the positive direction, while NH_2–SAM tends to shift in a negative direction, which is a clear indication of charge modulation on the channel by both SAMs. Let us take the case of the pentacene-based p-type OFET, in which the holes are the main charge carriers. After the functionalization, electron-donating NH_2 groups reduce the positive charge density on the channel, leading to a decrease in the drain current and a negative shift in the V_{th}. Conversely, CF_3 accumulates the positive charge on the surface of OFET due to its electron-withdrawing nature. Thus, the drain current increases and the V_{th} is positively shifted as extra voltage is needed to offset the enhanced positive surface charge. The author also argued that the polar SAMs molecules developed a built-in potential or electric field on the OFET due to the dipole alignment of the SAM molecules, consequently modulating the devices performance. This effect is similar to the way SAMs can modify the work function of metals.[78]

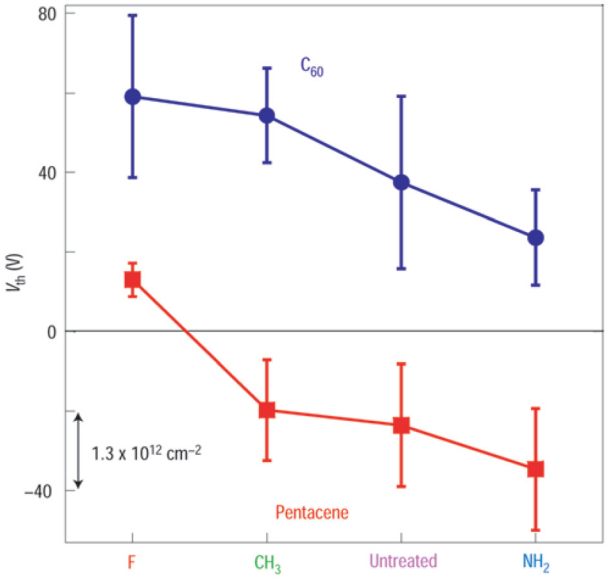

Fig. 4 Summary of the threshold voltage V_{th} in n-type C_{60} and p-type pentacene TFT devices for different SiO_2 treatments, untreated, and with three kinds of SAMs. The plots represent the averaged values over three to six devices; the error bars indicate the standard deviation. The scale indicates that the difference in V_{th} of 20 V corresponds to the carrier density of 1.3 × 10^{12} cm^{-2}, as estimated using the thickness and dielectric constant of the SiO_2 gate insulator. Reproduced from ref. 67 with permission from Nature Springer, copyright 2004.

However, later in the review of the literature, we will see that functionalization of APTES whose terminal group is NH_2 tends to decrease the baseline conductance of the n-type ZnO

Table 1 Advantages and disadvantages of the Dip and CVD methods

Dip method		Chemical vapor deposition	
Advantage	Disadvantage	Advantage	Disadvantage
Simple and cost-effective	Limited control over uniformity	High uniformity of SAM layer	Required specialized equipment
Ease of scalability	Time-consuming	High purity	Often involves elevated temperatures
Does not require specialized equipment Flexible for the mixing of SAMs	Require a surface that does not degrade when dipped in the solvent	Offering higher control over the deposition parameters	Limited compatibility with some substrates

This journal is © The Royal Society of Chemistry 2025

Open Access Article. Published on 20 bezna 2025. Downloaded on 29.05.2026 23:13:50.
This article is licensed under a Creative Commons Attribution 3.0 Unported Licence.

nanowires by pushing the electron away from the surface. This is in contrast to the work done by S. Kobayashi *et al.*,[67] in which NH_2–SAM tends to accumulate electrons on the surface. The molecular dipoles calculated through simulation in this report were not able to explain the electron accumulation by NH_2–SAM. The author reported an alternative hypothesis whose basis is the direct charge transfer between NH_2–SAM and organic semiconductors. This indicates that the effect of polar SAM molecules on surface charge density is still not clear, especially on semiconductor surfaces. On the other hand, tuning the work function of metal electrodes at the metal/semiconductor interface *via* the orientation of SAM dipoles presents a rather clear picture of how SAM tunes the surface charge density.[79] Fig. 5(a–c) showed basically three stages: i. metal/semiconductor interface without SAM (Fig. 5a) and ii. with SAM functionalization, as shown in Fig. 5(b and c). Φ_e represents the electron injection barrier, *i.e.*, energy difference between the metal work function and the lowest unoccupied molecular orbital (LUMO) of an organic semiconductor. In Fig. 5b, the SAM molecular dipole aligns in a way that its negative pole is facing the metal, while the positive end is facing away from the metal. This creates an electric field that pulls upward, hence decreasing the work function and also Φ_e. *Vice versa* is true for Fig. 5c. Following this work, SAM functionalization of metal electrodes proves to be highly beneficial in enhancing the performance of OFETs,[80,81] organic light-emitting diodes (OLEDs)[82,83] and solar cells[84,85] *via* modifying the injection barriers.

These results collectively show that surface charge density can be modulated by employing polar SAM molecules. This modulation holds particular promise for nanostructured metal oxide (MOX)-based sensors, where gas-sensing interactions occur at the surface. Since the sensing interactions are fundamentally driven by electron donation or extraction, tuning the surface charge density can enhance the sensing performance (discussed in section 3).[46,48,59,60] Beyond surface charge modulation, SAM terminal groups were also found to participate in direct charge transfer with gas analytes, further boosting the sensor performance.[59] However, this mechanism requires additional investigation, particularly through *in situ* gas sensing measurements.

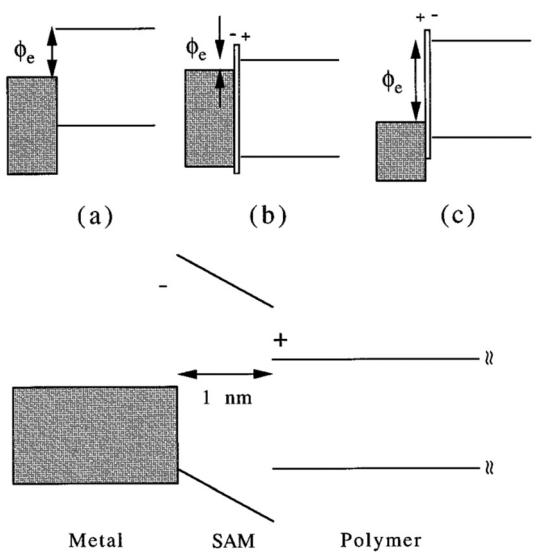

Fig. 5 Schematic energy level diagrams of metal/organic interfaces: panel a, untreated interface; panel b and panel c, dipole layer which decreases and increases the electron Schottky energy barrier, respectively; and panel d, magnified view of the interface. Reproduced from ref. 79 with permission from American Physical Society, copyright 1996.

3. Progress in the development of SAMs-functionalized MOXs gas sensors

As compared to other strategies such as decoration with metal particles and heterostructures, only a limited amount of work has been reported on SAMs-functionalized MOXs gas sensors. In this section, we will review all the reported work on SAM-functionalized MOXs gas sensors. This section is divided into two sub-sections, *i.e.*, SAM-functionalized n-type and p-type MOXs. Additionally, within each of these sub-sections, the effect of SAM functionalization on the sensing performance of different MOXs are individually discussed.

3.1. SAM functionalized n-type metal oxides

3.1.1. Tin dioxide (SnO_2). The first noticeable report was published by Hoffman *et al.*[48] on a highly selective room-temperature NO_2 sensor based on SnO_2 nanowires (NWs) functionalized with self-assembled monolayers (SAMs) of *N*-[3-(trimethoxysilyl)propyl]ethylenediamine (en-APTAS). Unlike typical metal oxide sensors that rely on thermal activation, this sensor utilized solar light as a source of activation, operating at room temperature. To fabricate the SAM-modified sensing device, SnO_2 NWs were deposited on an alumina substrate, pre-patterned with interdigitated gold contacts, as shown in Fig. 6. The SnO_2 NWs were then immersed in a 1% solution of en-APTAS in ethanol and stirred for 6 hours, ensuring uniform SAM functionalization. The terminal groups of en-APTAS are $–NH_2$ (amine), which led to the development of amine-terminated SnO_2 NW sensors. The NWs' 1D morphology, characterized by high surface-to-volume ratios and abundant active sites, provided a robust platform for gas adsorption and interaction.

The performance of the fabricated sensor was evaluated under solar light illumination (85 mW cm^{-2}), as depicted in Fig. 7. The results revealed highly selective behavior toward NO_2, even at a low concentration of 0.4 ppm, with a sensitivity of 2100% as compared to other gases such as SO_2, NH_3, and CO, which showed negligible responses. Furthermore, the selectivity of the sensors was attributed to the interaction between the NO_2 molecules and the amine groups of SAM. The electron-donating nature of the amine groups facilitates charge transfer to the electron-withdrawing NO_2, thereby

Open Access Article. Published on 20 bezna 2025. Downloaded on 29.05.2026 23:13:50.
This article is licensed under a Creative Commons Attribution 3.0 Unported Licence.

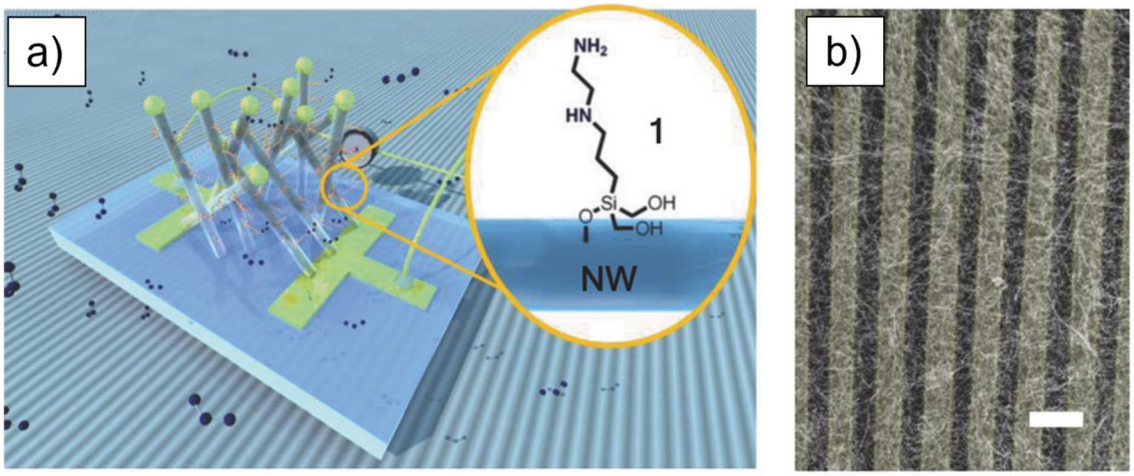

Fig. 6 (a) Schematic of the selective NO_2 sensor. *N*-[3-(Trimethoxysilyl)propyl]ethylenediamine (en-APTAS 1) was immobilized on the surface of SnO_2 NWs, which were directly grown on an interdigital gold electrode (5 μm spacings). The measured device resistance served as the sensor signal. (b) Scanning electron microscope (SEM) image of the en-APTAS **1** modified SnO_2 NWs with an average diameter of 47 ± 8 nm, grown on an interdigital electrode (scale bar, 10 μm). Reproduced from ref. 48 with permission from Wiley, copyright 2014.

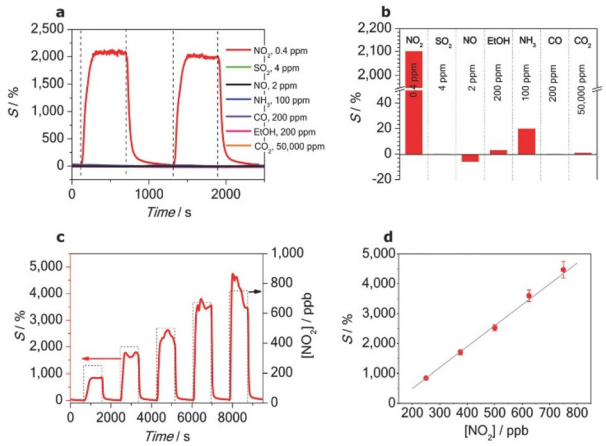

Fig. 7 en-APTAS **1** functionalized SnO_2 NW sensor measured under solar illumination (85 mW cm^{-2}). (a) Pulses of 0.4 ppm NO_2, SO_2 (4 ppm), NO (2 ppm), NH_3 (100 ppm), ethanol (200 ppm), CO (200 ppm) and CO_2 (50 000 ppm). (b) Summary of sensitivities towards the tested gases. (c) Sensing response *vs.* different NO_2 concentrations ranging from 250 to 750 ppb in synthetic air. (d) Linear behaviour of the sensor response with different NO_2 concentrations. Reproduced from ref. 48 with permission from Wiley, copyright 2014.

causing a significant increase in the sensor resistance and modulating the sensor response.

In addition, Fig. 8 reports on the theoretical insights obtained through density functional theory (DFT) simulations, which revealed that the alignment of the lowest unoccupied molecular orbital (LUMO) of NO_2 with the Fermi level of the SAM-functionalized SnO_2 NWs was critical for achieving this selectivity. This alignment optimized the charge transfer process, reinforcing the sensor's high sensitivity and selectivity. Despite its success, the study also highlights challenges such as maintaining sensor stability under humid conditions and addressing potential signal saturation during prolonged NO_2 exposure. These findings underscore the need for further optimization of the SAM-functionalized sensors, particularly for real-world applications. Nonetheless, this work represents a milestone in leveraging nanoscale phenomena to advance MOX-based gas sensors, showcasing the potential of SAM-functionalized 1D nanostructures for highly selective and low-temperature gas detection.

Furthermore, a report published by Park *et al.*[58] focused on SnO_2 nanowire (NW) sensors functionalized with self-assembled monolayers (SAMs) for the selective detection of various volatile organic compounds (VOCs). The SnO_2 NWs were functionalized with four different SAMs (alkyl, fluoroalkyl, alkylthiol, and alkylammonium) to explore their effects on the sensor performance and selectivity. The SnO_2 NWs were synthesized using a vapor–liquid–solid (VLS) method, and subsequently functionalized through a dip-coating process after oxygen plasma treatment in a Diener Electronic Pico (200 W, 40 kHz) setup, which enhanced the surface's hydroxyl content.

The SAM-functionalized SnO_2 NW sensors demonstrated enhanced selectivity and optimal performance at a reduced operating temperature of 175 °C, which is lower than the typical operating temperatures for similar MOX-based sensors. However, the response magnitude was somewhat limited, with a value of around 2.86 for 50 ppm of CH_4. Notably, the authors observed a shift in the selective response of the sensor toward different VOCs depending on the type of SAM used for functionalization, as shown in Fig. 9(a–e). The selective sensing mechanism hinges on the interaction between specific functional groups in the SAMs and the target gas molecules. Each SAM functional group promotes non-covalent interactions such as van der Waals, electrostatic, or dipolar interactions, which favor the adsorption of target gas molecules.

 This journal is © The Royal Society of Chemistry 2025

Open Access Article. Published on 20 bezna 2025. Downloaded on 29.05.2026 23:13:50.
This article is licensed under a Creative Commons Attribution 3.0 Unported Licence.

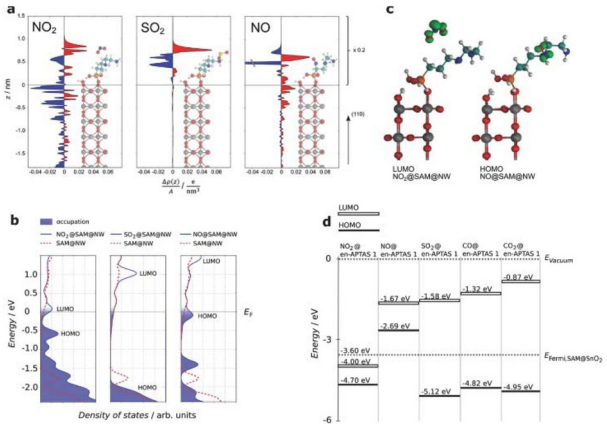

Fig. 8 (a) Change in the averaged one-dimensional charge density $\Delta\rho(z)$ per surface area A along the (110) direction upon NO_2, SO_2 and NO adsorption on the en-APTAS **1** functionalized SnO_2 (110) surface for the energetically most favourable geometries. These geometries are shown as insets, and are true to length scale. The electron charge is denoted by e. Regions of charge depletion are indicated by blue, and regions of charge accumulation are indicated by red fillings. For clarity, $\Delta\rho(z)$ has been scaled by a factor of 0.2 in the region outside of SnO_2. The SnO_2 surface (z = 0) is defined by the average position of the bridging oxygen atoms on the SnO_2 surface along the (110) direction. (b) Density of states (DOS) of the en-APTAS **1** modified SnO_2 with adsorbed NO_2, SO_2 and NO. The Fermi levels of the different systems are set to 0 eV. For comparison, the DOS of the en-APTAS **1** modified SnO_2 NW without an adsorbed gas molecule (dashed red line) is shown in each graph. (c) Charge densities of the wave functions corresponding to the peaks in the densities of states aligned with the Fermi levels from b are shown as green isosurfaces. The isosurfaces are drawn at a value of 0.075 e Å^{-3}. These are basically the LUMO of the NO_2 molecule, and the HOMO of the NO molecule. (d) Energy diagram of the frontier orbitals of the two- and three-atomic gases adsorbed on en-APTAS **1**. Gases with HOMOs below and LUMOs above the Fermi level of the SAM-modified SnO_2 do not lead to a noticeable gas sensing signal in the experiments. NO_2 with the LUMO of the NO_2-en-APTAS **1** system below the Fermi level leads to an increasing sensor resistance, whereas NO with the HOMO being above the Fermi level leads to a decreasing sensor resistance. Reproduced from ref. 48 with permission from Wiley, copyright 2014.

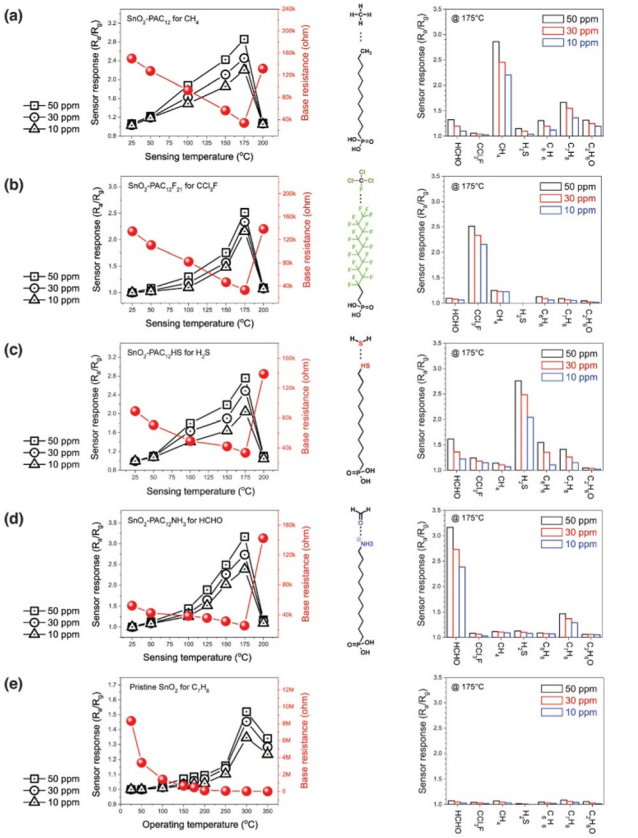

Fig. 9 Sensor responses and corresponding selectivity patterns of (a) PAC_{12}-functionalized, (b) $PAC_{12}F_{21}$-functionalized, (c) $PAC_{12}HS$-functionalized, (d) $PAC_{12}NH_3$-functionalized, and (e) pristine SnO_2 NWs gas sensors with respect to various concentrations of gas, along with the base resistance as a function of the sensing temperature. The representative molecular interactions between each SAM molecule and the corresponding gas molecules are plotted in the middle. Reproduced from ref. 58 with permission from Elsevier, copyright 2021.

For instance, the thiol groups in the alkylthiol SAM show high affinity for H_2S, while the alkylammonium SAM facilitates dipolar interactions with HCHO. The molecular dynamics (MD) simulations revealed that the interaction between the SAM functional groups and target gases altered the depletion layer width of the SnO_2 NWs, ultimately changing the sensor's resistance. Notably, the base resistance of the SAM-functionalized sensors was reduced, which improved their sensitivity to target gases. Overall, this report provides valuable insights into how SAM modification can create a tunable platform for the selective detection of various gas analytes.

Furthermore, in a similar work, Park *et al.*[86] have again functionalized the SnO_2 NWs with different SAMs, *i.e.*, 1-methyl-3-(dodecylphosphonic acid)imidazolium bromide ($PAC_{12}IMI$), 10-carboxydecylphosphonic acid ($PAC_{10}CA$), and (2-{2-[2-methoxy–ethoxy]-ethoxy}-ethyl)phosphonic acid (PAG_3). The motivation behind this work was to establish the relationship between the SAMs chemical structures and their preferential gas-sensing behaviors. On the basis of experimental findings, the author argued that the intermolecular interactions between SAM molecules and gas analytes determine the preferred sensing behaviour. For instance, ionically charged moieties were selective towards C_3H_6O, while alkyl chains were more interactive with CH_4 and C_7H_8 gases.

3.1.2. Tungsten oxide (WO_3). Explorations into functionalizing n-type MOXs with SAMs have extended to tungsten oxide (WO_3), where WO_3-based sensors have shown promising results in gas sensing. Liu *et al.*[47] developed a NO_2 sensor using WO_3 nanotubes (NTs) functionalized with 3-aminopropyltriethoxysilane (APTES) to enhance the selectivity and sensitivity for NO_2 detection. The WO_3 NTs were synthesized *via* electrospun polymer nanofibers as sacrificial templates, which were soaked and calcined to produce thin-walled, porous NT structures (Fig. 10). Furthermore, X-ray photoelectron spectroscopy (XPS) provided critical insights into the surface chemistry of pristine and APTES-functionalized WO_3 NTs (Fig. 10(h–k)). High-resolution W 4f spectra confirmed the

Open Access Article. Published on 20 bezna 2025. Downloaded on 29.05.2026 23:13:50.
This article is licensed under a Creative Commons Attribution 3.0 Unported Licence.

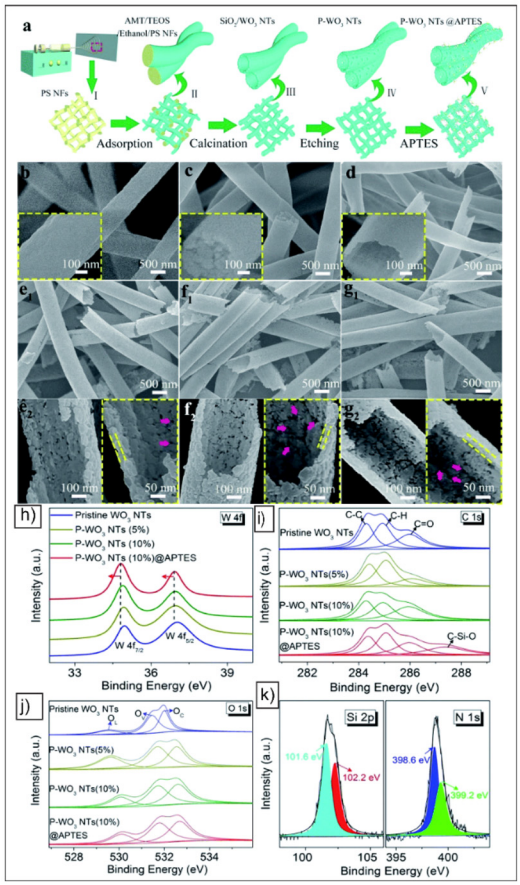

Fig. 10 (a) Schematic of the synthetic process for APTES functionalized porous WO_3 NTs. The SEM images of the (b) as-spun PS nanofibres, (c) AMT/TEOS/PS composite nanofibres, and (d) SiO_2/WO_3 composite NTs. (e_1) SEM image and (e_2) corresponding magnifications of P–WO_3 NTs (5%). (f_1) SEM image and (f_2) corresponding magnifications of P–WO_3 NTs (10%). (g_1) SEM image and (g_2) corresponding magnifications of P–WO_3 NTs (10%)@APTES. The inset images in panels (b), (c) and (d) are the corresponding magnifications. (h) W 4f, (i) C 1s, and (j) O 1s XPS spectra of the pristine WO_3 NTs, P–WO_3 NTs (5%), P–WO_3 NTs (10%) and P–WO_3 NTs (10%)@APTES samples. (k) Si 2p and N 1s XPS spectra of the P–WO_3 NTs (10%)@APTES sample. Reproduced from ref. 47 with permission from RSC, copyright 2018.

presence of W^{6+} in WO_3, with peaks at 35.2 and 37.3 eV. A shift to lower binding energies after APTES modification indicated increased oxygen vacancies (OVs), known to enhance adsorption properties. In the C 1s spectra, functionalization introduced a peak at 287.8 eV, corresponding to the C–Si–O bond, confirming APTES attachment. The O 1s spectra revealed surface lattice oxygen (OL), oxygen vacancies (OV), and chemisorbed oxygen (OC), with the latter increasing significantly from 10.7% in pristine WO_3 NTs to 25.8% in the APTES-modified sample. This rise in OC is critical for improved gas-sensing interactions. Additionally, Si 2p and N 1s spectra confirmed the formation of Si–O–W and Si–O–Si bonds on the WO_3 surface, with N–H and C–N peaks verifying the presence of terminal amine groups. These findings indicate that APTES forms stable covalent bonds with WO_3 NTs, while leaving the amine group available for interaction with analytes. The APTES-functionalized WO_3 NTs (P–WO_3 NTs (10%)) exhibited a highly enhanced response to NO_2, with a 23-fold increase in sensitivity towards 1 ppm of NO_2 at the optimal working temperature of 340 °C compared to unmodified WO_3 NTs (Fig. 11a). Furthermore, APTES also introduces hydrophobic properties, helping the sensor maintain high performance even in humid environments. Specifically, the responses of the P–WO_3 NTs (APTES 10%) sensors only decreased from 45 to 36.4 with the RH% increase from 25% to 90% (Fig. 11c). The NTs were then functionalized with varying concentrations of APTES (5 and 10 mol%) to investigate the impact of the SAM density on the sensing performance. The APTES-functionalized WO_3 NTs (P–WO_3 NTs (10%)) exhibited a highly enhanced response to NO_2, with a 23-fold increase in sensitivity towards 1 ppm of NO_2 at the optimal working temperature of 340 °C compared to unmodified WO_3 NTs (Fig. 11(a and b)). Furthermore, APTES also introduces hydrophobic properties, helping the sensor maintain high performance even in humid environments (Fig. 11d). Specifically, the responses of the P–WO_3 NTs (APTES 10%) sensors only decreased from 45 to 36.4 with the RH% increase from 25 to 90% (Fig. 11c).

The sensing performance of the P–WO_3 NTs (10%)@APTES sensor was enhanced through effective APTES modification, including an ultra-high response and exceptional selectivity toward NO_2 (Fig. 11). The response of the sensor was up to 23 times higher than that of pristine WO_3 NTs, with a low detection limit of 10 ppb. It demonstrated rapid response and recovery times of 11 s and 12 s, respectively, for 10 ppm NO_2, achieving a response value of 184. Additionally, the sensor showed excellent long-term stability, maintaining performance even under high humidity conditions. The improved sensing performance is attributed to the dual structural and electronic effects introduced by APTES functionalization. The amine

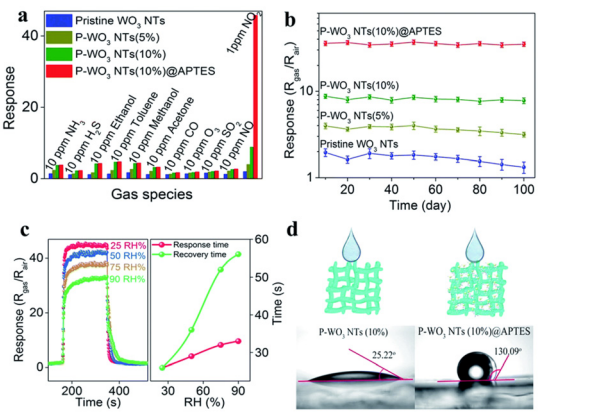

Fig. 11 (a) Selectivity and (b) stability tests for the pristine WO_3 NTs, P–WO_3 NTs (5%), P–WO_3 NTs (10%) and P–WO_3 NTs (10%)@APTES gas sensors at the corresponding operating temperature. (c) Dynamic curves of the P–WO_3 NTs (10%)@APTES sensor at different RH% (25%–90%) for 1 ppm NO_2. (d) Water contact angles of the P–WO_3 NTs (10%) and P–WO_3 NTs (10%)@APTES on glass substrates. Reproduced from ref. 47 with permission from RSC, copyright 2018.

This journal is © The Royal Society of Chemistry 2025

Open Access Article. Published on 20 bezna 2025. Downloaded on 29.05.2026 23:13:50.
This article is licensed under a Creative Commons Attribution 3.0 Unported Licence.

groups of APTES act as electron donors, selectively enhancing the interaction of an electron-withdrawing gas like NO_2. This selective interaction enhances charge transfer at the sensor surface, increasing the depletion layer and resulting in a pronounced rise in resistance upon NO_2 exposure. Additionally, creating a porous, highly interactive surface, the APTES-functionalized WO_3 NTs enable greater gas adsorption, facilitating more effective and selective NO_2 detection at lower concentrations.

Furthermore, in a recent study, Tomić *et al.*[60] reported on UV light-activated sensors based on WO_{3-x} NWs modified with APTES for detecting gases like ethanol and nitrogen dioxide (NO_2) at room temperature. The WO_3 NWs were synthesized using aerosol-assisted chemical vapor deposition (AACVD) and then functionalized with APTES *via* a controlled chemical vapor deposition process. The APTES-modified WO_3 NWs (APTES@WO_{3-x}) demonstrated distinct sensing enhancements under UV illumination, providing a significant alternative to temperature-based activation (Fig. 12). The APTES@WO_{3-x} sensors exhibited improved sensing response under UV-light, achieving an approximate 17-fold increase in sensitivity to ethanol and a 20-fold increase to NO_2 compared to non-functionalized WO_{3-x} sensors (Fig. 12(a and b)). Operating at room temperature with UV irradiation at 365 nm (up to 1800 mW cm^{-2}), the APTES@WO_{3-x} sensors detected ethanol and NO_2 at concentrations as low as 10 ppm, and demonstrated rapid response and recovery times. The UV activation enabled the sensors to maintain high baseline stability and consistent performance across extended operation periods of up to 560 hours (Fig. 12(c and d)).

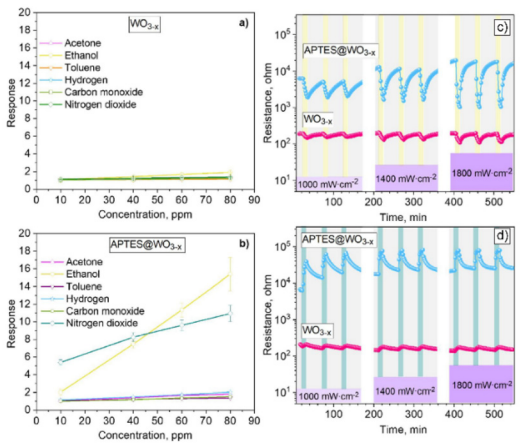

Fig. 12 Dependence of the response on the gas concentration for the sensors based on (a) WO_{3-x} and (b) APTES@WO_{3-x}. The calibration curves display the mean of the response and the standard error of the mean obtained using four different sensors of each type and at least three replicates for each tested condition. Typical resistance changes for the sensors based on WO_{3-x} and APTES@WO_{3-x} sensors to 80 ppm of (c) ethanol and (d) nitrogen dioxide and various radiant flux. The yellow and green bars represent the on–off for ethanol and nitrogen dioxide, respectively. Reproduced from ref. 60 with permission from Elsevier, copyright 2021.

Explaining the sensing mechanism, the functionalization with APTES introduces reactive amine groups that facilitate the adsorption and interaction with ethanol and NO_2 molecules, particularly under UV illumination (Fig. 13(a–d)). The sensing mechanism, as described by the authors, involves two stages: initial photo-activation and subsequent gas interaction. In the first stage, the UV light excites the WO_{3-x} surface, which leads to the generation of electron–hole pairs. This excitation activates the adsorbed oxygen species, forming more reactive oxygen ions (O_2^-), which create a stable depletion layer that primes the sensor surface for gas exposure (Fig. 13(a–c)). In the second stage, when ethanol or NO_2 is introduced, these gases interact with the photo-induced oxygen ions, resulting in charge transfer reactions that alter the resistance of the WO_{3-x} NWs. For ethanol (a reducing gas), interaction with the oxygen ions releases electrons back into the WO_{3-x} NW, reducing resistance (Fig. 13d). In the case of NO_2 (an oxidizing gas), the interaction with the oxygen ions depletes electrons, leading to an increase in resistance. Furthermore, the strong selectivity to ethanol among other reducing gases is attributed to the reactive amino group at the APTES@WO_{3-x} sensors, which facilitates the reaction with the tested gases. Finally, these UV-driven mechanisms allow for highly sensitive and selective gas detection at room temperature without the need for high thermal energy, marking a promising step forward for energy-efficient gas sensor technology.

3.1.3. Zinc oxide (ZnO). Furthermore, in an article published by Singh *et al.*,[46] the authors developed SAM-functiona-

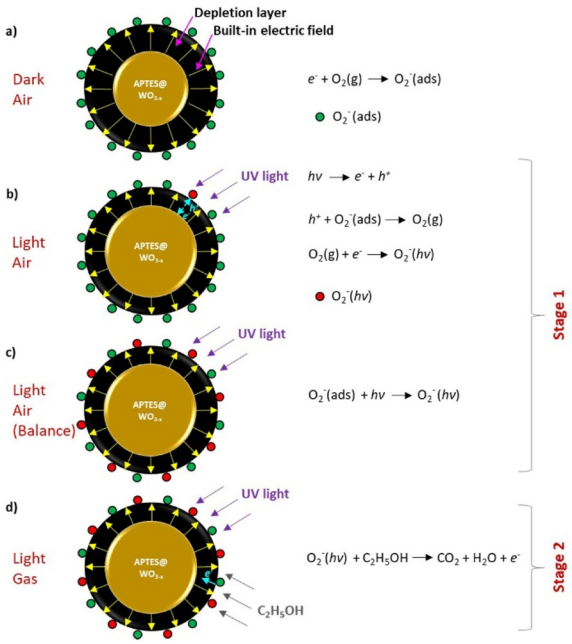

Fig. 13 Schematic of the gas-sensing mechanism of the UV-LED-activated, APTES-modified WO_{3-x} sensor under different conditions: (a) exposed to dry air in the dark, (b) exposed to dry air under UV light, (c) exposed to dry air under UV light after achieving oxygen adsorption/desorption balance, (d) exposed to ethanol under UV light. Reproduced from ref. 60 with permission from Elsevier, copyright 2021.

Open Access Article. Published on 20 bezna 2025. Downloaded on 29.05.2026 23:13:50.
This article is licensed under a Creative Commons Attribution 3.0 Unported Licence.

lized ZnO nanowire (NW) sensors for the selective detection of acetone in exhaled breath, specifically targeting applications in the diagnosis of diabetes. The ZnO NWs were synthesized using a vapor–liquid–solid (VLS) mechanism, which resulted in nanowires of dense morphology with a diameter of 10–20 nm. The functionalization of the ZnO NWs was carried out using two different SAMs: (3-aminopropyl)trimethoxysilane (APTMS or APTES) and 3-glycidoxypropyltrimethoxysilane (GLYMO or GOPS), as shown in Fig. 14(a–c). The ZnO NWs were immersed in 10×10^{-3} M solutions of APTMS and GLYMO in ethanol for 18 hours, during which time the SAM molecules covalently bonded to the ZnO surface *via* siloxane linkages (Si–O–Si). This process generated two types of functionalized surfaces: amino-terminated ($-NH_2$) for APTMS and epoxy-terminated for GLYMO. Additionally, X-ray photoelectron spectroscopy (XPS) analysis was used to confirm the successful functionalization of the ZnO NWs (Fig. 14(d–i)). The C 1s spectra showed an increased intensity of the C–O bond (at BE = 286.4 eV) in the APTMS and GLYMO samples compared to bare ZnO, indicating the presence of SAMs on the surface. Additionally, the N 1s peak was observed only in the APTMS-functionalized sample, confirming the presence of amino groups, while the oxygen 1s spectra also reflected the expected chemical changes due to functionalization. Furthermore, the gas-sensing performance of both bare and SAM-functionalized ZnO NW sensors was evaluated at different temperatures and for the gas analyst (Fig. 15(a and b)). Notably, the APTMS-functionalized sensors exhibited a fivefold higher response than bare ZnO NWs at 300 °C, while the GLYMO-functionalized sensors showed a threefold improvement. The detection limits were significantly enhanced by SAM functionalization, with the APTMS-modified ZnO NW sensors showing a detection limit of as low as 0.5 ppm, making them ideal for acetone detection in exhaled breath.

The gas-sensing mechanism of the SAM-functionalized ZnO NWs relies on the interaction of acetone molecules with surface-adsorbed oxygen ions (Fig. 15c). In bare ZnO NWs, oxygen adsorbs onto the surface, extracting electrons from the conduction band, creating an electron depletion layer (EDL) and increasing the sensor resistance. When exposed to acetone (a reducing gas), the acetone donates electrons to the ZnO NWs, reducing the resistance. In APTMS-functionalized

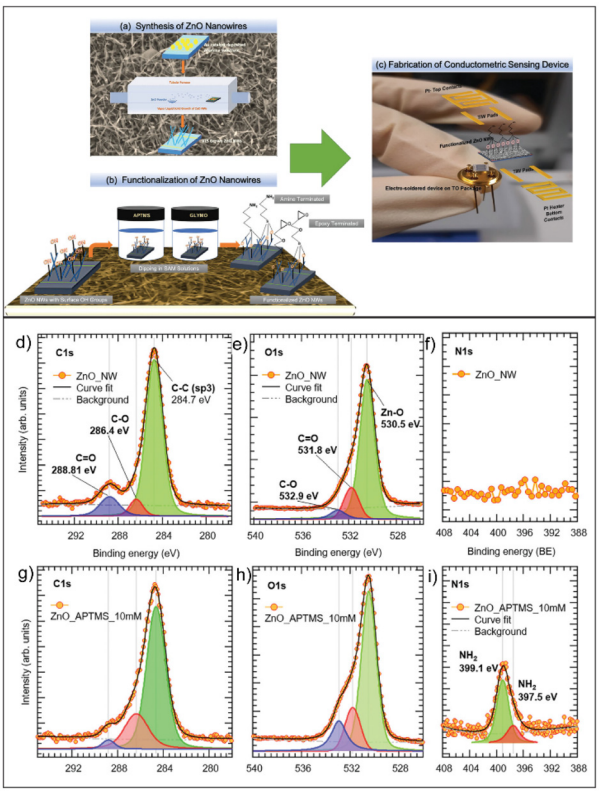

Fig. 14 (a) Synthesis of ZnO nanowires using the vapor–liquid–solid (VLS) mechanism, (b) surface functionalization of ZnO nanowires with APTMS and GLYMO self-assembled monolayers, and (c) conductometric sensing device. (d–f) XPS spectra for bare ZnO NW (first row), (g–i) APTMS (second row). Reproduced from ref. 46 with permission from Wiley, copyright 2020.

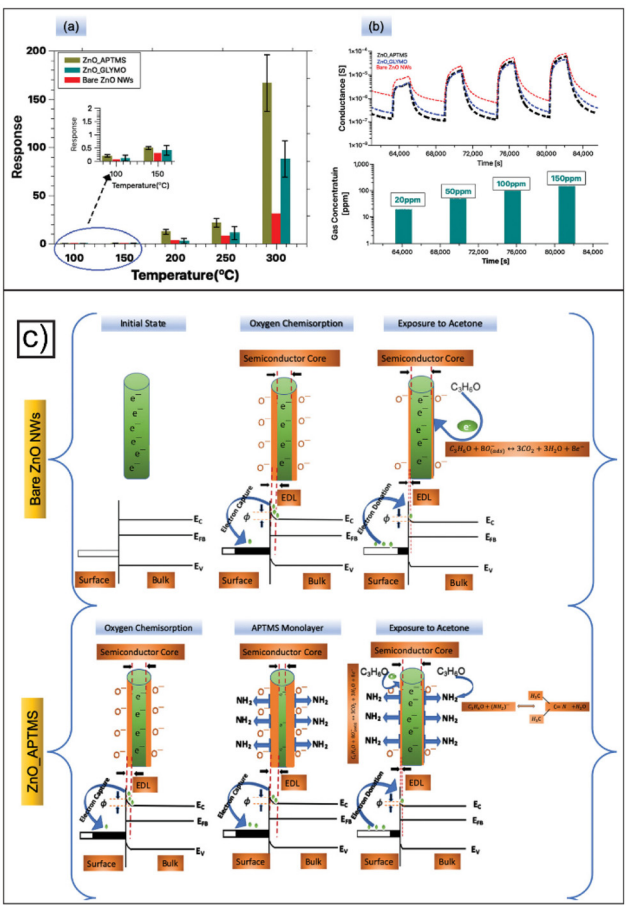

Fig. 15 (a) Response *versus* temperature plot. (b) Dynamic response (at 300 °C) of bare and SAM (10×10^{-3} m APTMS and GLYMO) functionalized ZnO nanowires recorded in dry air. (c) Gas-sensing mechanism of bare and SAM (10×10^{-3} m APTMS) functionalized ZnO NWs for acetone detection. Reproduced from ref. 46 with permission from Wiley, copyright 2020.

This journal is © The Royal Society of Chemistry 2025

Open Access Article. Published on 20 bezna 2025. Downloaded on 29.05.2026 23:13:50.
This article is licensed under a Creative Commons Attribution 3.0 Unported Licence.

ZnO NWs, the amine groups enhance this interaction. The $-NH_2$ groups react with acetone, forming imine and water, further boosting electron transfer and sensor response. This reaction, combined with the wider EDL in SAM-modified ZnO NWs, results in the improved sensing performance that is observed.

Similar to this work, recently, Singh *et al.*[87] have reported on the selective detection of hydrogen (H_2) with APTES-functionalized ZnO NWs at 200 °C. The underlying sensing mechanism is explained based on the negatively charged $-NH_2$ groups of APTES that pushed the electron away from the surface, this making the surface more favorable for reducing gases like hydrogen that donates electrons. These results indicate that the selectivity of APTES functionalized ZnO NWs can be tuned with the operational temperature.

Furthermore, Singh *et al.*[59] investigated the methyl-terminated ZnO NW sensors functionalized with tetraethyl orthosilicate (TEOS) for selective acetone detection. Similar to the previous report, the ZnO NWs were fabricated using the VLS mechanism and the dip method was used to functionalize the NWs with TEOS. The TEOS-functionalized ZnO NWs demonstrated superior performance with a notable improvement in response and selectivity when compared to bare ZnO NWs towards acetone (Fig. 16(a–d)). The sensor response increased by three-fold, with the optimal working temperature reduced to 250 °C compared to the previously reported APTES–ZnO NWs sensors. More specifically, the response of the functionalized and bare ZnO NWs was found to be 170 ± 21.6 and 66.7, respectively, toward 50 ppm of acetone, as shown in Fig. 16a. Indeed, the TEOS-functionalized sensor exhibited a detection limit of 1 ppm at 250 °C, making them a promising candidate for applications like exhaled breath analysis. Additionally, even in the presence of humidity, the sensor retained approximately 50% of its response (Fig. 16d), underscoring its robustness in real-world environments. Discussing the sensing mechanism, the author described the enhancement in the sensing performance as attributed to the interaction between the methyl groups ($-CH_3$) of the TEOS SAM and the carbonyl group (C═O) of acetone (Fig. 16f). The intermolecular interactions lead to an efficient transfer of electrons, causing a modulation in the surface electron density of the ZnO NWs. This modulation amplifies the sensor response by reducing the electron depletion layer when acetone molecules interact with the surface of ZnO NWs. Additionally, weak van der Waals interactions between the methyl groups of TEOS and acetone further contribute to the selective response of the sensor, reinforcing its potential for high-performance acetone detection in complex environments.

Meanwhile, in bare ZnO nanowires, the reaction between adsorbed O^- ions and acetone molecules lead to the change in the conductance of the sensor (Fig. 16e). However, in TEOS functionalized sensors, the nucleophilic–electrophilic intermolecular interactions between the terminal $-CH_3$ groups of TEOS and C═O (carbonyl group) of acetone cause the modulation in the surface electron density of nanowires, and hence enhance the response. In addition to this, weak interactions between the methyl groups of TEOS and acetone participate in enhancing the sensor selectivity.

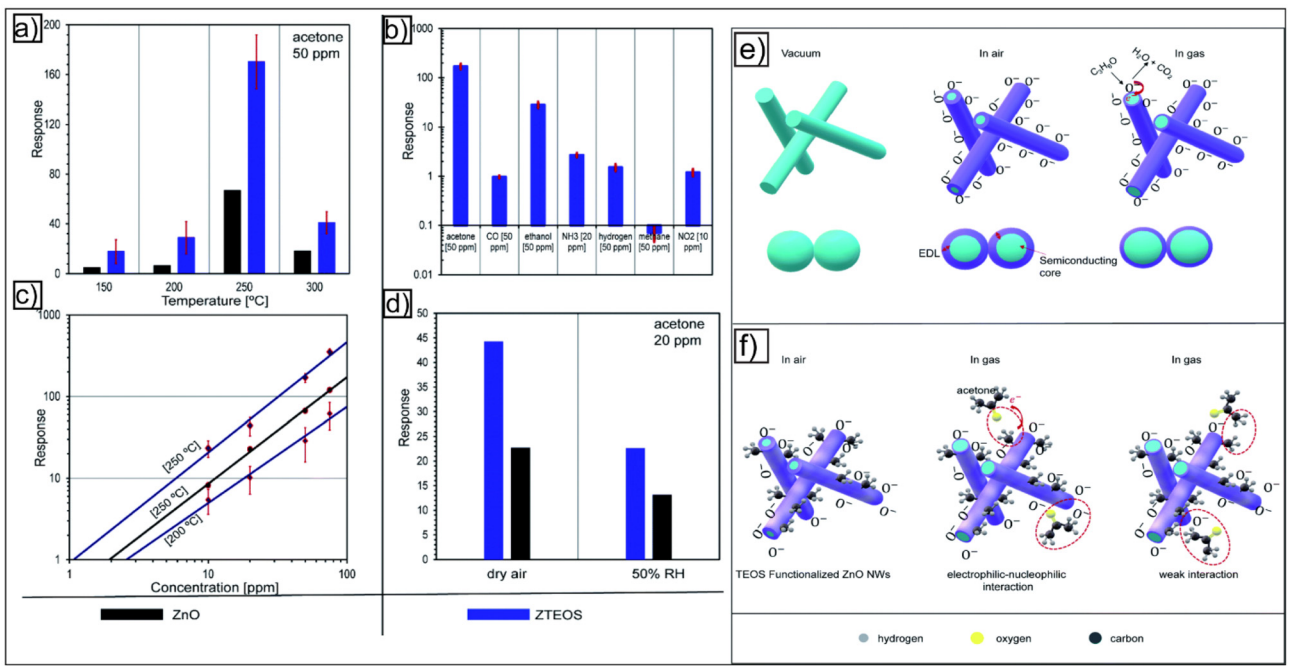

Fig. 16 (a) Response *vs.* temperature graph of the bare and TEOS-functionalized ZnO NWs for 50 ppm acetone in dry air. (b) Response of the TEOS-functionalized ZnO NWs toward acetone and other interfering gases at 250 °C in dry air. (c) Calibration curves of bare and TEOS-functionalized ZnO NWs for acetone at 200 °C and 250 °C. (d) Effect of humidity on the bare and TEOS-functionalized ZnO NW response. Gas-sensing mechanism of (e) bare and (f) TEOS-functionalized ZnO nanowires for acetone. Reproduced from ref. 59 with permission from RSC, copyright 2022.

Open Access Article. Published on 20 bezna 2025. Downloaded on 29.05.2026 23:13:50.
This article is licensed under a Creative Commons Attribution 3.0 Unported Licence.

Additionally, a recent report by Singh *et al.*[51] introduced an innovative approach for tailoring the surface chemistry of ZnO nanowires (NWs) for selective acetone detection by using a mixed self-assembled monolayer (mixed-SAM) strategy. The ZnO NWs as shown in Fig. 17(a and b) were functionalized with varying ratios ($AP_1:TS_3$ (1 : 3), $AP_1:TS_1$ (1 : 1) and $AP_3:TS_1$ (3 : 1)) of two SAMs: (3-aminopropyl)triethoxysilane (APTES) and tetraethyl orthosilicate (TEOS). Using this mixed SAM approach, the authors modified the surface characteristics of ZnO to adjust its sensitivity and selectivity toward acetone. An XPS investigation confirmed the successful functionalization, revealing the presence of Si and N in the mixed-SAM samples, specifically associated with the $-CH_3$ and $-NH_2$ groups of TEOS and APTES, respectively (Fig. 17(c–r)). The XPS spectra indicated distinct changes in the carbon, oxygen, and nitrogen peaks, corresponding to the mixed functional groups on the ZnO surface, further validating the mixed SAM structure and its uniform attachment on ZnO NWs.

The mixed SAM-functionalized ZnO NW sensors demonstrated the highest response towards acetone, with an optimal response at 300 °C, as shown in Fig. 18(a and b). Among different mixing ratios, the sensor with a 1 : 1 ratio of APTES and TEOS (referred to as AP1 : TS1) showed a highly selective

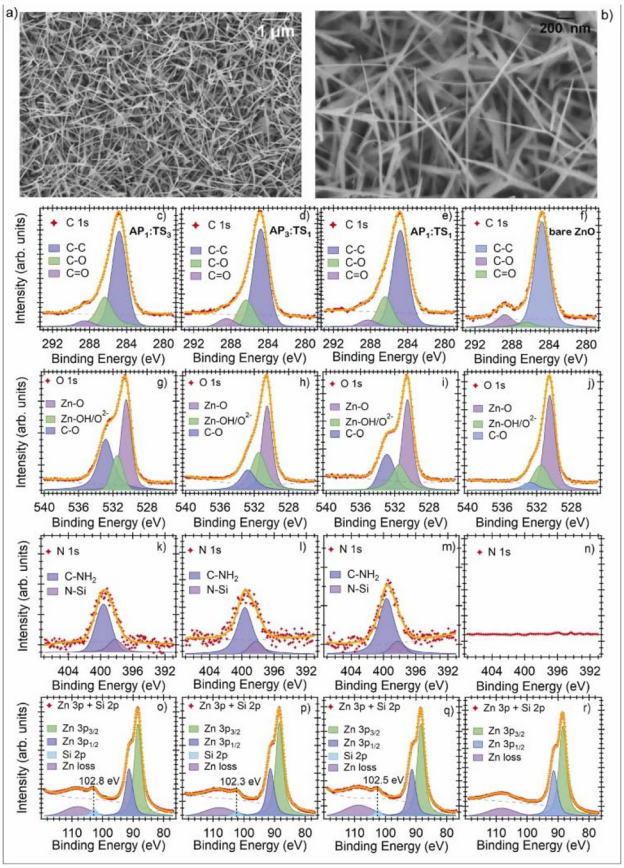

Fig. 17 (a, b) SEM images of the bare ZnO NWs at different magnifications. XPS spectra of: C 1s (c–f), O 1s (g–j), N 1s (k–n), Zn 3p and Si 2p (o–r). Red markers denote the experimental trace, the orange line is the fit, and the dashed line is the background. The Voigt peaks are included under each spectrum, along with their physical interpretation. ZnO data. Reproduced from ref. 51 with permission from Elsevier, copyright 2023.

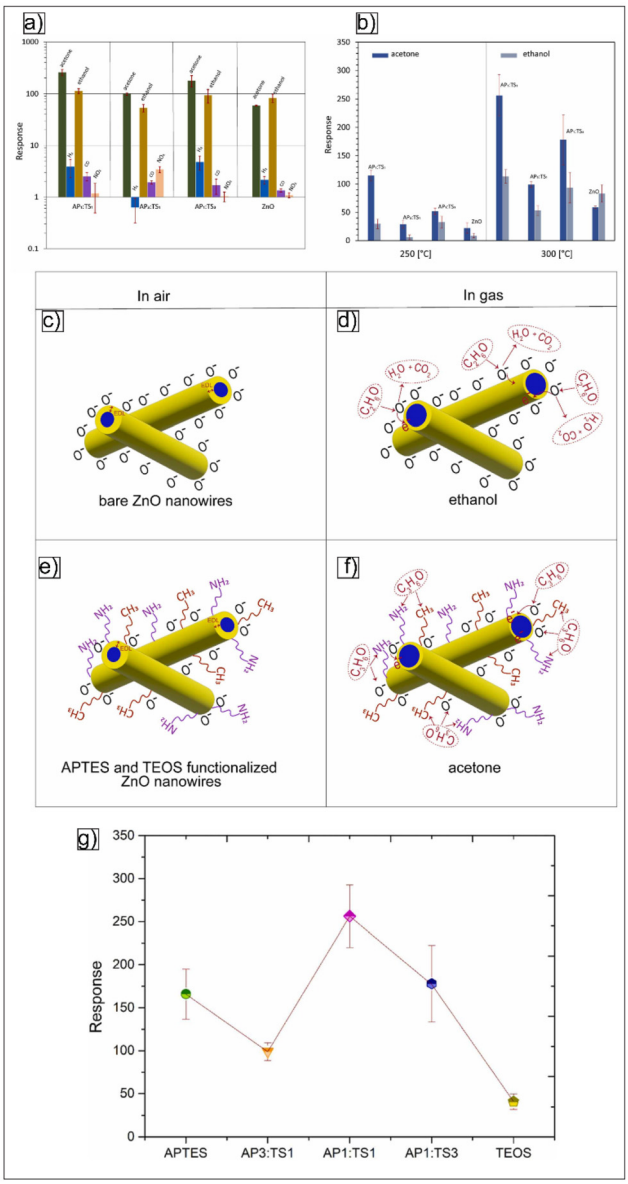

Fig. 18 (a) Selectivity of sensors toward acetone and ethanol at 300 °C. (b) Comparison of the response toward acetone (50 ppm) and ethanol (50 ppm) at 250 °C and 300 °C in a linear scale. Acetone sensing mechanism of bare and mixed-SAMs functionalized sensors. (c) Chemisorbed O– ions on bare ZnO nanowires surface in air. (d) Interactions of chemisorbed oxide ions with acetone. (e) Surface chemical composition of mixed-SAMs functionalized ZnO nanowires. (f) Electrophilic–nucleophilic interaction between the C═O group of acetone and terminal-SAMs groups ($-CH_3$ and $-NH_2$). (g) Effect of the mixing ratio on the performance of SAMs-functionalized ZnO nanowires acetone sensors. To fully understand this phenomenon, we have considered the results of our previous works, in which the ZnO nanowires were functionalized with homogenous APTES and TEOS monolayers. In all of the cases, the response toward 50 ppm of acetone at 300 °C under dry conditions was considered. Reproduced from ref. 51 with permission from Elsevier, copyright 2023.

This journal is © The Royal Society of Chemistry 2025

Open Access Article. Published on 20 bezna 2025. Downloaded on 29.05.2026 23:13:50.
This article is licensed under a Creative Commons Attribution 3.0 Unported Licence.

response of 256 ± 36 towards 50 ppm of acetone compared to other interfering gases (Fig. 18a), with the calculated lowest detection limit of 0.05 ppm. Additionally, as observed from the XPS analysis, the optimal 1 : 1 SAM mixture promoted a balanced charge distribution, which provides a positive influence on the gas interaction and sensor response. The sensing mechanism here is similar to prior reports by Singh, involving the interaction between the carbonyl (C═O) group of acetone and the terminal groups of the SAMs (Fig. 18(e and f)). Specifically, the $-CH_3$ (from TEOS) and $-NH_2$ (from APTES) groups act as nucleophilic centers, facilitating electron-donating interactions with acetone. Interestingly, the study found that varying the SAM mixing ratio significantly impacted the sensor response. Particularly, in Fig. 18g, the performance of the mixed-SAM functionalized sensor is compared with that of the mono-SAM. These results clearly indicate that the mixed-SAM is a superior strategy compared to functionalization with mono-SAM, provided that the mixing ratio is carefully chosen. The 1 : 1 mixture provided an optimal charge distribution on the ZnO NW surface, enhancing interactions with acetone molecules, and thus improving the selectivity and response. This mixing ratio tuning allowed the sensor to achieve a highly stable response over two months, indicating strong potential for real-world applications like exhaled breath analysis. This report underscores the potential of mixed SAM strategies as a highly customizable approach to achieving selective gas sensors by altering the surface interaction dynamics.

3.2. SAM functionalized p-type (NiO) metal oxide

We have seen from the literature and discussion in the previous section (3.1) that the SAMs functionalization strategy has been extensively applied to the n-type MOXs to enhance their sensitivity and selectivity for VOCs and other gases. In contrast, the application of SAMs to p-type MOXs-based sensors remains largely unexplored. In fact, p-type MOXs are still relatively less explored and underdeveloped in gas sensing, as compared to n-type MOXs. The reason behind this is their poor charge-transport and electrical properties. Briefly speaking, the chemisorption of oxygen on p-type MOXs creates a narrow hole-accumulation layer (HAL) around the resistive core. As the charge transport occurs in this narrow HAL, p-type MOXs exhibit limited charge in electrical resistance/conductance upon interaction with the gas analyte, leading to their poor sensing performance. To achieve relatively better sensing performance, p-type MOXs generally need to operate at significantly higher temperature (300–500 °C). In order to tackle this issue, Kaur *et al.*[50] functionalized NiO nanowires (NWs) with organosilane (3-glycidoxypropyltrimethoxysilane (GOPS)), marking the first reported use of SAMs for the functionalization of a p-type MOX-based sensor. The goal of this study was to improve the gas-sensing performance of NiO NWs by modulating the surface charge carrier concentration by functionalization to detect reducing gases, such as ethanol and acetone at a lower operating temperature (Fig. 19). The GOPS-functionalized NiO (NGP) sensors demonstrate detection limits as low as 0.9 ppm for ethanol and 2 ppm for acetone at an optimal operating temperature of 200 °C. Remarkably, the response values for GOPS-functionalized NiO were approximately 9 times greater than those of bare NiO NWs when tested with ethanol and acetone at this lower temperature (Fig. 19(b–f)). In contrast, bare NiO NWs required a higher temperature of 500 °C to achieve comparable responses (Fig. 19g), underscoring the advantage of SAM functionalization in enabling effective sensing at reduced temperatures. In the case of pristine NiO NWs, the interactions between reducing gases and chemisorbed O^- ions were found to define their sensing mechanism and performance (Fig. 19ii). Meanwhile, in the case of NGP nanowires, the GOPS introduced negatively charged epoxy end-groups on the NiO surface, which facilitated relatively more hole accumulation near the nanowire surface as compared to pristine NiO NWs, creating an environment that is more favorable to electron acceptance from reducing gases like ethanol and acetone at 200 °C (Fig. 19(iii–v)). Hence, when the NGP sensors were exposed to ethanol and acetone at 200 °C, the enhanced electron transfer occurs between the analyte and NiO NWs, which leads to a higher response value.

This pioneering work marks a significant advancement in the field of p-type MOX functionalization with SAMs, laying a promising foundation for the future development of low-temperature gas sensors based on NiO devices. However, further investigation is needed to enhance the sensor selectivity and its ability to distinguish effectively between different VOCs.

4. Major challenges

Clearly, after reviewing the comprehensive literature, SAM functionalization represents an excellent strategy to fabricate future-generation ultrasensitive, miniaturized and low-power consuming sensor for environment/health monitoring. However, there are still some major challenges to overcome to make use of their full potential.

The first and most prominent issue is of fundamental character, *i.e.*, to understand the interactions of SAM with MOXs and gas analytes. The discussion presented in section 2.3 shows how the molecular dipole or polar SAM molecules modulate the surface charges. This theory explained the change in the work-functional of metals, but it does not fully explain the change in the performance of semiconductor devices like OFET. Recalling the results of S. Kobayashi *et al.*,[67] a shift in the threshold-voltage was clearly seen that signifies the charge modulation on the OFET channel after the functionalization with SAM having NH_3 and CF_3 polar end-groups. The dipole moment of these SAM predicted *via* theoretical DFT calculations has not been able to explain the change modulation, and then electrochemical doping theory was partially employed to explain the results. This clearly showed the complex nature of interactions between SAMs and semiconductors that are not fully understood. This is attributed to the more complex electronic properties of semiconducting

Open Access Article. Published on 20 bezna 2025. Downloaded on 29.05.2026 23:13:50.
This article is licensed under a Creative Commons Attribution 3.0 Unported Licence.

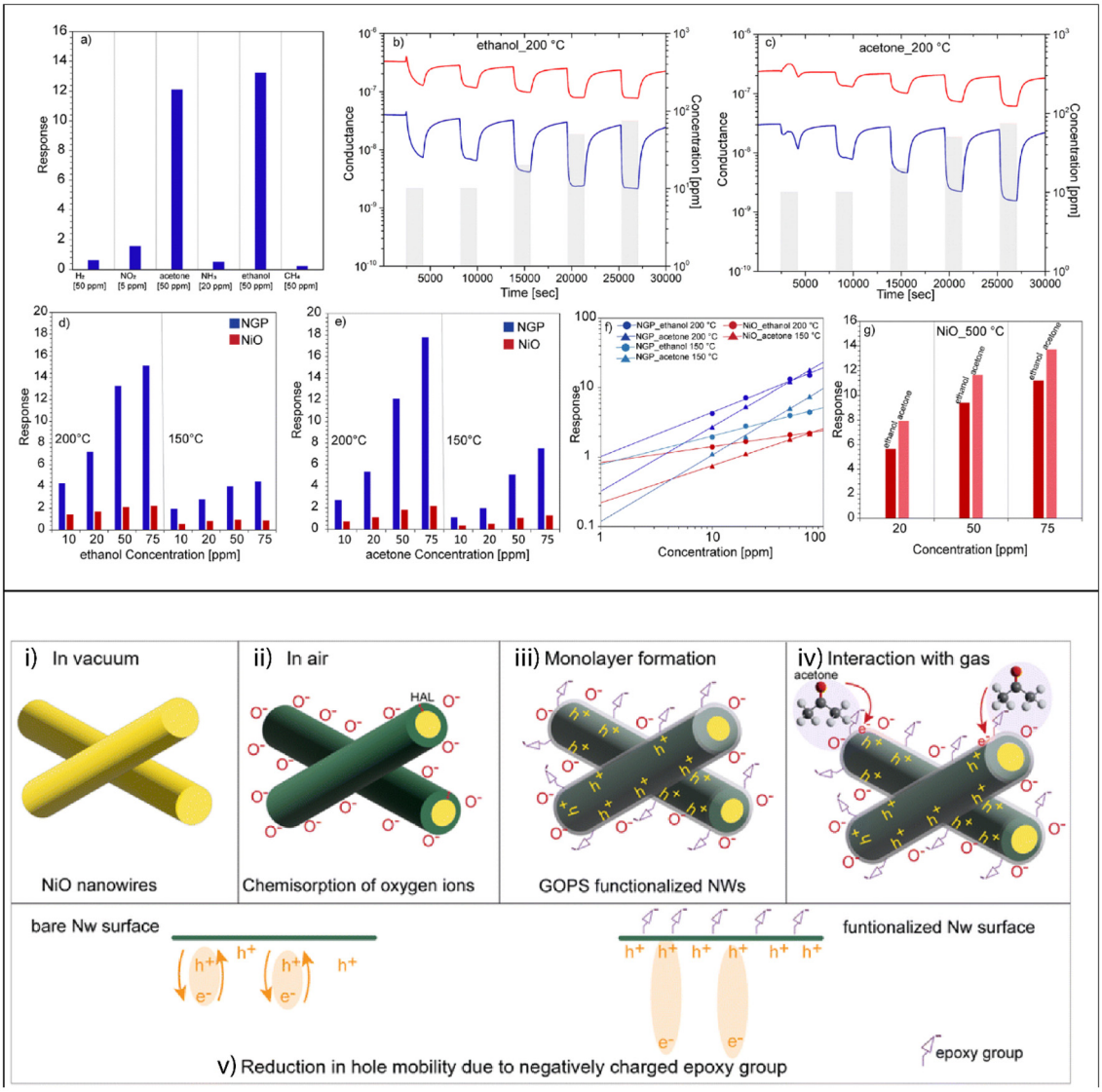

Fig. 19 (a) Response of the NGP sensor toward different gas analytes. (b and c) Dynamic response of NiO (red) and NGP (blue) sensors toward the different concentrations of ethanol and acetone (10, 10, 20, 50, and 75 ppm) in dry air at 200 °C. (d and e) Response *vs.* concentration curves of bare NiO and NGP at 200 °C and 150 °C toward ethanol and acetone. (f) Calibration curves of the NiO and NGP sensors for ethanol and acetone. (g) Response *vs.* concentration graph of the NiO sensor toward ethanol and acetone at 500 °C. (i) NiO nanowires in a vacuum. (ii) Chemisorption of oxygen ions (O^-) occurs on the surface of NiO NWs, which leads to the formation of a narrow hole accumulation layer (HAL) around the resistive core. (iii) Monolayer formation on the NWs surface that leads to the accumulation of holes near the surface due to the presence of negatively charged epoxy groups of GOPS. (iv) Enhanced interaction with acetone gas leads to an increase in electron–hole recombination as compared to bare NiO NWs. (v) Reduction in the hole mobility occurs after the functionalization with GOPS. Reproduced from ref. 50 with permission from RSC, copyright 2023.

materials from metal. In the case of metals, their electronic properties are mainly determined by the high density of free charge carries ($\sim 10^{23}$ cm^{-3})[31] due to the overlap between the valence and conduction band (zero-band gap).[88] Meanwhile, in the case of semiconductor materials, the conduction (CB) and valence bands (VB) are well separated, *i.e.*, the existence of a band-gap.[89] Their electronic properties are not only determined by the presence of free charge carriers in their CB or VB, but also by many other factors such as the band-gap, surface defects, impurities, *etc.*[90–92] The situation can be further complicated if the doping has been employed to tune their electronic properties, which leads to the modification in their band structure and introduction of several defects.[93] Hence, in the case of semiconductors, one should consider not only the interaction between the free charge carriers, but also with other entities such as defects. As far as the molecular interactions between SAMs end-groups and gas analyte are concerned, no experimental observation has been reported especially in the case of sensing, even though these types of interactions are chemically possible and exist.

This journal is © The Royal Society of Chemistry 2025

Open Access Article. Published on 20 bezna 2025. Downloaded on 29.05.2026 23:13:50.
This article is licensed under a Creative Commons Attribution 3.0 Unported Licence.

The other major challenges are specific to the sensing. (i) Stability under high-temperature and humid conditions is one of the primary concerns with SAMs and their stability under extreme conditions, such as high temperatures and high humidity. Gas sensors based on MOX materials often require operating temperatures of 200 °C–400 °C to achieve optimal sensitivity and response times.[13] However, SAMs, being organic in nature, tend to degrade at elevated temperatures, which can compromise their functionality and lead to sensor failure over time. Furthermore, with regards to their stability under higher humid environments, the interaction of water molecules with the MOX surface or SAM molecules can disrupt the functional groups, weaken the bond between the SAM layer and MOX surface, and result in poor sensor performance over time.[46] (ii) Limitation in achieving multi-gas selectivity: while SAM functionalization can significantly improve selectivity towards specific gases, achieving multi-gas selectivity remains a complex challenge. Many SAMs are designed to target a single class of analytes[46,50,51,59] based on specific functional groups, limiting their applicability in detecting multiple gases simultaneously. Moreover, in real-world environments, gas sensors are exposed to complex mixtures of gases, making it difficult to distinguish target gases from interfering species accurately. This limitation underscores the need for advanced functionalization strategies, such as combining SAMs with other selective coatings or integrating machine learning algorithms to enhance the selectivity. Furthermore, concerning the functionalization techniques, (iii) the reproducibility and uniformity in SAM formation are often challenging due to variations in deposition techniques and the sensitivity of SAM formation to parameters, such as the solution concentration, temperature, and substrate properties. Any irregularity in SAM formation can lead to inconsistencies in the sensor performance and limit the scalability for commercial applications.[46] (iv) Stability and long-term performance of the prepared sensors. The stability of SAM-functionalized sensors is another critical challenge, as prolonged exposure to harsh conditions, such as oxidizing environments or contaminants, can lead to the gradual degradation of SAMs. This degradation may result in reduced sensitivity and selectivity of the sensing devices over time.

5. Future directions

By considering the major challenges, future directions should be focused on understanding the SAM interactions with semiconductors and gas analytes as far as the fundamental aspect of SAM is concerned. This requires coupled theoretical and advanced experimental studies. By unraveling the fundamental nature of these interactions, further optimization of the sensor performance can be achieved.

On the other hand, to further improve the stability of SAMs under extreme conditions, multi-gas selectivity, structural uniformity of monolayer, *etc*., these can be combined with the future efforts in designing and synthesizing novel SAM molecules. These novel SAMs molecules should be designed especially for sensing applications, so that these drawbacks of the sensor can be improved.

6. New opportunities

Even though some major challenges still needed to be addressed, surface functionalization represents an exceptional new way to address the long-standing challenges of MOXs, *i.e.*, to improve their selectivity and lower the working temperature. To address the issue of high-temperature operation, the use of light (photo-activation) as a source of activation instead of temperature is one step forward.[3] However, the current state-of-the-art research studies show that most of the work in this direction was done on n-type MOXs, and these photo-activated sensors showed better performance mainly toward oxidizing gases like NO_2.[3] Our work on SAM functionalization shows that by selecting appropriate SAM molecules, this approach was found to be highly efficient for the detection of reducing gases with both n- and p-type MOXs. Hence, by adopting SAM functionalization, the performance of these photoactivated sensors can be further improved toward reducing gas compounds.

Furthermore, an important insight from the above work is that the SAM-functionalized WO_3 nanotubes[47] retained strong sensing performance even under extremely high humidity conditions. This is attributed to the unique property of SAMs like APTES, which enable manipulation of surface wettability. In addition to enhancing the sensing performance, SAM functionalization has gained significant attention for its role in controlling the surface wettability and improving hydrophobicity.[94,95] Humidity interference, or "humidity poisoning"[96] is a long-standing challenge in MOX-based gas sensors. By applying SAMs to the sensor surface, this issue can be effectively mitigated. For example, Z. K. He *et al.*[97] demonstrated that SAM-modified CeO_2/TiO_2 nanotube arrays maintained high sensitivity toward ammonia under humid conditions. Therefore, SAM functionalization offers a promising strategy to improve gas sensor performance in high-humidity environments and represents a valuable pathway for the development of next-generation sensors.

7. Conclusions

In summary, our comprehensive review of literature has proved the potential and efficiency of SAM functionalization of MOXs sensors in addressing their long-standing issues of lack of selectivity and high-temperature operation. Modulation of surface charges and SAMs/gas analyte molecular interactions were found to be the main reasons behind the improvement in the sensing performance. Especially, the selectivity of the n-type MOXs have vastly improved after SAMs functionalization, owing to the molecular-interactions between the analytes and SAMs end-groups. On the other hand, lowering the

Open Access Article. Published on 20 bezna 2025. Downloaded on 29.05.2026 23:13:50.
This article is licensed under a Creative Commons Attribution 3.0 Unported Licence.

working temperature of p-type NiO NWs from 500 °C to 200 °C *via* surface functionalization with organosilanes for the detection of reducing compounds is a great accomplishment. Further work needs to be done for the selective detection of these compounds. By coupling these improvements in both n- and p-type MOXs sensors with photoactivated sensors, we believe that future-generation portable, miniaturized, robust and low-power consuming sensors can be developed for healthcare and environment monitoring.

Data availability

This review article uses results that have already been published.

Conflicts of interest

There are no conflicts of interest to declare.

Acknowledgements

The authors would like to acknowledge the SENSOR Laboratory, Department of Information Engineering (DII), University of Brescia and IMEM-CNR, Trento for their support.

References

1 C. Wei, Z. Guo, H. Wang, S. Zhang, D. Hao and J. Huang, *Mater. Horiz.*, 2025, **12**, 317–342.
2 N. Kaur, M. Singh, A. Moumen, G. Duina and E. Comini, *Materials*, 2020, **13**, 2974.
3 R. Kumar, X. Liu, J. Zhang and M. Kumar, *Nano-Micro Lett.*, 2020, **12**, 164.
4 T. Islam, S. C. Mukhopadhyay and N. K. Suryadevara, *IEEE Sens. J.*, 2017, **17**, 577–584.
5 L. Portilla, K. Loganathan, H. Faber, A. Eid, J. G. D. Hester, M. M. Tentzeris, M. Fattori, E. Cantatore, C. Jiang, A. Nathan, G. Fiori, T. Ibn-Mohammed, T. D. Anthopoulos and V. Pecunia, *Nat. Electron.*, 2023, **6**, 10–17.
6 R. A. Potyrailo, *Chem. Rev.*, 2016, **116**, 11877–11923.
7 Y. Gu, B. Huang and H. Zhu, *IEEE Sens. J.*, 2024, **1**, 2125–2140.
8 M. Kavitha, D. S. H. Raju, S. F. Waris and D. A. Koulagaji, *IOP Conf. Ser.: Mater. Sci. Eng.*, 2020, **981**, 22003.
9 A. Mirzaei, S. G. Leonardi and G. Neri, *Ceram. Int.*, 2016, **42**, 15119–15141.
10 E. Comini, *Anal. Chim. Acta*, 2006, **568**, 28–40.
11 T. Li, W. Zeng and Z. Wang, *Sens. Actuators, B*, 2015, **221**, 1570–1585.
12 D. R. Miller, S. A. Akbar and P. A. Morris, *Sens. Actuators, B*, 2014, **204**, 250–272.
13 N. Kaur, M. Singh and E. Comini, *Adv. Mater. Interfaces*, 2022, 2101629.
14 N. Kaur, M. Singh and E. Comini, *Langmuir*, 2020, **36**, 6326–6344.
15 H.-T. Jung, *ACS Sens.*, 2022, **7**, 912–913.
16 B. Saruhan, R. Lontio Fomekong and S. Nahirniak, *Front. Sens.*, 2021, **2**, DOI: **10.3389/fsens.2021.657931**.
17 E. Comini, C. Baratto, I. Concina, G. Faglia, M. Falasconi, M. Ferroni, V. Galstyan, E. Gobbi, A. Ponzoni, A. Vomiero, D. Zappa, V. Sberveglieri and G. Sberveglieri, *Sens. Actuators, B*, 2013, **179**, 3–20.
18 S. K. T. Thathsara, C. J. Harrison, R. K. Hocking and M. Shafiei, *Int. J. Hydrogen Energy*, 2022, **47**, 18208–18227.
19 E. Espid and F. Taghipour, *Crit. Rev. Solid State Mater. Sci.*, 2017, **42**, 416–432.
20 F. Xu and H.-P. Ho, *Micromachines*, 2017, **8**, 333.
21 A. Chizhov, M. Rumyantseva and A. Gaskov, *Nanomaterials*, 2021, **11**, 892.
22 M. Šetka, M. Claros, O. Chmela and S. Vallejos, *J. Mater. Chem. C*, 2021, **9**, 16804–16827.
23 Q. Geng, Z. He, X. Chen, W. Dai and X. Wang, *Sens. Actuators, B*, 2013, **188**, 293–297.
24 L. Han, D. Wang, J. Cui, L. Chen, T. Jiang and Y. Lin, *J. Mater. Chem.*, 2012, **22**, 12915–12920.
25 C. Zhang, A. Boudiba, P. De Marco, R. Snyders, M.-G. Olivier and M. Debliquy, *Sens. Actuators, B*, 2013, **181**, 395–401.
26 P. Chakrabarty, M. Banik, N. Gogurla, S. Santra, S. K. Ray and R. Mukherjee, *ACS Omega*, 2019, **4**, 12071–12080.
27 I. Kriegel, F. Scotognella and L. Manna, *Phys. Rep.*, 2017, **674**, 1–52.
28 J. J. Goings, A. M. Schimpf, J. W. May, R. W. Johns, D. R. Gamelin and X. Li, *J. Phys. Chem. C*, 2014, **118**, 26584–26590.
29 S. Ghosh, M. Saha, S. Paul and S. K. De, *Small*, 2017, **13**, 1602469.
30 G. Bühler, D. Thölmann and C. Feldmann, *Adv. Mater.*, 2007, **19**, 2224–2227.
31 M. Singh, F. Scotognella and G. M. Paternò, *Mater. Adv.*, 2024, **5**, 6796–6812.
32 A. Agrawal, S. H. Cho, O. Zandi, S. Ghosh, R. W. Johns and D. J. Milliron, *Chem. Rev.*, 2018, **118**, 3121–3207.
33 H. Ji, W. Zeng and Y. Li, *Nanoscale*, 2019, **11**, 22664–22684.
34 A. Staerz, U. Weimar and N. Barsan, *Sens. Actuators, B*, 2022, **358**, 131531.
35 Y.-F. Sun, S.-B. Liu, F.-L. Meng, J.-Y. Liu, Z. Jin, L.-T. Kong and J.-H. Liu, *Sensors*, 2012, **12**, 2610–2631.
36 N. Goel, K. Kunal, A. Kushwaha and M. Kumar, *Eng. Rep.*, 2023, **5**, e12604.
37 C. W. Na, H. S. Woo and J. H. Lee, *RSC Adv.*, 2012, **2**, 414–417.
38 T. Jinkawa, G. Sakai, J. Tamaki, N. Miura and N. Yamazoe, *J. Mol. Catal. A: Chem.*, 2000, **155**, 193–200.
39 A. Kolmakov, D. O. Klenov, Y. Lilach, S. Stemmer and M. Moskovits, *Nano Lett.*, 2005, **5**, 667–673.
40 S. Park, G. J. Sun, H. Kheel, S. K. Hyun, C. Jin and C. Lee, *Met. Mater. Int.*, 2016, **22**, 156–162.

This journal is © The Royal Society of Chemistry 2025

Open Access Article. Published on 20 bezna 2025. Downloaded on 29.05.2026 23:13:50.
This article is licensed under a Creative Commons Attribution 3.0 Unported Licence.

41 Z. Lou, F. Li, J. Deng, L. Wang and T. Zhang, *ACS Appl. Mater. Interfaces*, 2013, **5**, 12310–12316.
42 Y. Wang, L. Liu, C. Meng, Y. Zhou, Z. Gao, X. Li, X. Cao, L. Xu and W. Zhu, *Sci. Rep.*, 2016, **6**, 33092.
43 J.-H. Kim, A. Katoch and S. S. Kim, *Sens. Actuators, B*, 2016, **222**, 249–256.
44 J. Zhang, X. Liu, L. Wang, T. Yang, X. Guo, S. Wu, S. Wang and S. Zhang, *Nanotechnology*, 2011, **22**(18), 185501.
45 F. Li, X. Gao, R. Wang, T. Zhang and G. Lu, *Sens. Actuators, B*, 2017, **248**, 812–819.
46 M. Singh, N. Kaur, G. Drera, A. Casotto, L. S. Ermenegildo and E. Comini, *Adv. Funct. Mater.*, 2020, **30**, 2003217.
47 W. Liu, L. Xu, K. Sheng, C. Chen, X. Zhou, B. Dong, X. Bai, S. Zhang, G. Lu and H. Song, *J. Mater. Chem. A*, 2018, **6**, 10976–10989.
48 M. W. G. Hoffmann, J. D. Prades, L. Mayrhofer, F. Hernandez-Ramirez, T. T. Järvi, M. Moseler, A. Waag and H. Shen, *Adv. Funct. Mater.*, 2014, **24**, 595–602.
49 M. Singh, N. Kaur and E. Comini, *J. Mater. Chem. C*, 2020, **8**, 3938–3955.
50 N. Kaur, M. Singh, A. Casotto, L. Sangaletti and E. Comini, *Chem. Commun.*, 2023, **59**, 1329–1332.
51 M. Singh, N. Kaur, A. Casotto, L. Sangaletti and E. Comini, *Sens. Actuators, B*, 2023, **384**, 133653.
52 X. Cheng, Y.-Y. Noh, J. Wang, M. Tello, J. Frisch, R.-P. Blum, A. Vollmer, J. P. Rabe, N. Koch and H. Sirringhaus, *Adv. Funct. Mater.*, 2009, **19**, 2407–2415.
53 M. Li, M. Liu, F. Qi, F. R. Lin and A. K.-Y. Jen, *Chem. Rev.*, 2024, **124**, 2138–2204.
54 O. Fenwick, C. Van Dyck, K. Murugavel, D. Cornil, F. Reinders, S. Haar, M. Mayor, J. Cornil and P. Samorì, *J. Mater. Chem. C*, 2015, **3**, 3007–3015.
55 N. K. Chaki and K. Vijayamohanan, *Biosens. Bioelectron.*, 2002, **17**, 1–12.
56 O. Seitz, P. G. Fernandes, R. Tian, N. Karnik, H.-C. Wen, H. Stiegler, R. A. Chapman, E. M. Vogel and Y. J. Chabal, *J. Mater. Chem.*, 2011, **21**, 4384–4392.
57 T. Wink, S. J. van Zuilen, A. Bult and W. P. van Bennekom, *Analyst*, 1997, **122**, 43R–50R.
58 H. Park, J.-H. Kim, D. Vivod, S. Kim, A. Mirzaei, D. Zahn, C. Park, S. S. Kim and M. Halik, *Nano Today*, 2021, **40**, 101265.
59 M. Singh, N. Kaur, A. Casotto, L. Sangaletti, N. Poli and E. Comini, *J. Mater. Chem. A*, 2022, **10**, 3178–3189.
60 M. Tomić, Z. Fohlerova, I. Gràcia, E. Figueras, C. Cané and S. Vallejos, *Sens. Actuators, B*, 2021, **328**, 129046.
61 B. Zhang, T. Kong, W. Xu, R. Su, Y. Gao and G. Cheng, *Langmuir*, 2010, **26**, 4514–4522.
62 M. F. Calhoun, J. Sanchez, D. Olaya, M. E. Gershenson and V. Podzorov, *Nat. Mater.*, 2008, **7**, 84–89.
63 P. Böhme, G. Vedantham, T. Przybycien and G. Belfort, *Langmuir*, 1999, **15**, 5323–5328.
64 A. Hasan, V. Saxena and L. M. Pandey, *Langmuir*, 2018, **34**, 3494–3506.
65 D. Samanta and A. Sarkar, *Chem. Soc. Rev.*, 2011, **40**, 2567–2592.
66 M. Y. Mulla, E. Tuccori, M. Magliulo, G. Lattanzi, G. Palazzo, K. Persaud and L. Torsi, *Nat. Commun.*, 2015, **6**, 6010.
67 S. Kobayashi, T. Nishikawa, T. Takenobu, S. Mori, T. Shimoda, T. Mitani, H. Shimotani, N. Yoshimoto, S. Ogawa and Y. Iwasa, *Nat. Mater.*, 2004, **3**, 317–322.
68 A. Ulman, *Chem. Rev.*, 1996, **96**, 1533–1554.
69 D. L. Allara, *Biosens. Bioelectron.*, 1995, **10**, 771–783.
70 A. Tlili, A. Abdelghani, S. Hleli and M. A. Maaref, *Sensors*, 2004, **4**, 105–114.
71 M. Dawood, *Durability of Steel Components strengthened with fiber-reinforced polymer (FRP) composites*, ed. V. Karbhari, Woodhead Publishing, 2014, pp. 96–114.
72 J. Dong, A. Wang, K. Y. S. Ng and G. Mao, *Thin Solid Films*, 2006, **515**, 2116–2122.
73 H. Sugimura, A. Hozumi, T. Kameyama and O. Takai, *Surf. Interface Anal.*, 2002, **34**, 550–554.
74 K. Hayashi, N. Saito, H. Sugimura, O. Takai and N. Nakagiri, *Langmuir*, 2002, **18**, 7469–7472.
75 S. Onclin, B. J. Ravoo and D. N. Reinhoudt, *Angew. Chem., Int. Ed.*, 2005, **44**, 6282–6304.
76 A. Hozumi, Y. Yokogawa, T. Kameyama, H. Sugimura, K. Hayashi, H. Shirayama and O. Takai, *J. Vac. Sci. Technol., A*, 2001, **19**, 1812–1816.
77 B. Sun, J. Pang, Q. Cheng, S. Zhang, Y. Li, C. Zhang, D. Sun, B. Ibarlucea, Y. Li, D. Chen, H. Fan, Q. Han, M. Chao, H. Liu, J. Wang, G. Cuniberti, L. Han and W. Zhou, *Adv. Mater. Technol.*, 2021, **6**, 2000744.
78 B. de Boer, A. Hadipour, M. M. Mandoc, T. van Woudenbergh and P. W. M. Blom, *Adv. Mater.*, 2005, **17**, 621–625.
79 I. Campbell, S. Rubin, T. Zawodzinski, J. Kress, R. Martin, D. Smith, N. Barashkov and J. Ferraris, *Phys. Rev. B: Condens. Matter Mater. Phys.*, 1996, **54**, R14321(R).
80 F. Zhang, B. Geng, X. Ding, C. Huang, A. Fan, S. Duan, R. Li, X. Ren and W. Hu, *Adv. Mater. Technol.*, 2023, **8**, 2300451.
81 P. Marmont, N. Battaglini, P. Lang, G. Horowitz, J. Hwang, A. Kahn, C. Amato and P. Calas, *Org. Electron.*, 2008, **9**, 419–424.
82 J. Lee, B.-J. Jung, J.-I. Lee, H. Y. Chu, L.-M. Do and H.-K. Shim, *J. Mater. Chem.*, 2002, **12**, 3494–3498.
83 H. Zheng, F. Zhang, N. Zhou, M. Sun, X. Li, Y. Xiao and S. Wang, *Org. Electron.*, 2018, **56**, 89–95.
84 S. K. Hau, Y.-J. Cheng, H.-L. Yip, Y. Zhang, H. Ma and A. K.-Y. Jen, *ACS Appl. Mater. Interfaces*, 2010, **2**, 1892–1902.
85 L. Zuo, Z. Gu, T. Ye, W. Fu, G. Wu, H. Li and H. Chen, *J. Am. Chem. Soc.*, 2015, **137**, 2674–2679.
86 H. Park and J.-H. Kim, *ACS Sens.*, 2025, **10**, 741–750.
87 M. Singh, N. Kaur and E. Comini, *Sensors*, 2024, **24**, 7011.
88 K. W. Böer and U. W. Pohl, *Bands and Bandgaps in Solids*, ed. K. W. Böer and U. W. Pohl, Springer International Publishing, Cham, 2018, pp. 243–302.

Open Access Article. Published on 20 bezna 2025. Downloaded on 29.05.2026 23:13:50.
This article is licensed under a Creative Commons Attribution 3.0 Unported Licence.

89 A. F. J. Levi, *Essent. Semicond. Laser Device Phys*, 2018, pp. 1–26.
90 R. H. Williams, *Surf. Sci.*, 1983, **132**, 122–142.
91 M. D. McCluskey and A. Janotti, *J. Appl. Phys.*, 2020, **127**, 190401.
92 T. Matsubara and Y. Toyozawa, *Prog. Theor. Phys.*, 1961, **26**, 739–756.
93 A. L. E. Boris and I. Shklovskii, *Electronic Properties of Doped Semiconductors*, Springer, Berlin, Heidelberg, 1st edn, 2012.
94 M. Liu, S. Wang and L. Jiang, *Nat. Rev. Mater.*, 2017, **2**, 17036.
95 L. Feng, S. Li, Y. Li, H. Li, L. Zhang, J. Zhai, Y. Song, B. Liu, L. Jiang and D. Zhu, *Adv. Mater.*, 2002, **14**, 1857–1860.
96 H. Chai, Z. Zheng, K. Liu, J. Xu, K. Wu, Y. Luo, H. Liao, M. Debliquy and C. Zhang, *IEEE Sens. J.*, 2022, **22**, 5470–5481.
97 Z.-K. He, K. Li, R. Kou, W. Zhang, J. Zhao, Z. Gao and Y.-Y. Song, *ACS Sens.*, 2024, **9**, 1014–1022.

This journal is © The Royal Society of Chemistry 2025